Master's thesis

NTNU
Norwegian University of Science and Technology
Faculty of Engineering
Department of Energy and Process Engineering

Halvor Herlyng

Optimization of Pipe Geometries with Entropy Production Minimization in Viscous Flow

Master's thesis in Mechanical Engineering
Supervisor: Øivind Wilhelmsen
Co-supervisor: Ailo Aasen and Krzysztof Banasiak
April 2022

NTNU
Norwegian University of Science and Technology

Halvor Herlyng

Optimization of Pipe Geometries with Entropy Production Minimization in Viscous Flow

Master's thesis in Mechanical Engineering
Supervisor: Øivind Wilhelmsen
Co-supervisor: Ailo Aasen and Krzysztof Banasiak
April 2022

Norwegian University of Science and Technology
Faculty of Engineering
Department of Energy and Process Engineering

NTNU
Norwegian University of
Science and Technology

Abstract

How to remedy the irreversibilities of the fluid flow in ejectors and perform optimal design of ejectors is not yet fully understood. Ejectors are versatile devices used in various energy processes to compress and expand fluids. Both Computational Fluid Dynamics and experimental studies have demonstrated potential for improvement in the performance of ejectors by altering their geometry. Few previous studies have investigated the use of non-equilibrium thermodynamics to optimize the geometry of ejectors. The theory of non-equilibrium thermodynamics can be applied to quantify the local and thus total entropy production in a process. The total entropy production can be used to design energy-efficient process equipment with optimization, because energy-efficient processes are characterized by low entropy production.

In this thesis, the entropy production in pipe flow has been investigated. This was motivated by the thermodynamic irreversibilities of flow in ejectors. The working hypothesis of the thesis is that there exists an optimal radius profile for a circular pipe, in the sense that the profile minimizes the entropy production of the flow. A cross-sectional averaged one-dimensional model of viscous, adiabatic, single-phase air flow in a pipe of varying cross section has been developed. The theory of non-equilibrium thermodynamics has been applied to derive the local entropy production in the flow. Numerical optimization and optimal control theory were used for optimization of the radius profile of the pipe wall. The objective was to minimize total entropy production in the pipe. The fluid dynamic model and the optimization problems formulated were implemented and solved numerically. Numerical analyses and a thermodynamic consistency check were performed to validate all results.

Numerical constrained optimization solutions that converged to a local minimum were obtained. These solutions yielded radius profiles that reduced the total entropy production by 60% when compared to a reference case. The shape of the radius profiles was assessed to be inapplicable to pipe flow due to the radius profiles leading to detrimental three-dimensional flow features not accounted for in the model developed. Therefore, the reduction potential observed is characterized as unrealistic.

Furthermore, an optimal control theory optimization problem for the pipe flow was formulated with the slope of the radius profile as a control variable. The problem was implemented and attempted solved iteratively, but to no avail. The Hamiltonian of the problem disproved correctness of a result provided by the iterative solver used, but the physics of the solution was consistent with the fluid dynamic model developed. It was noted that the resulting radius profile reduced the total entropy production by 45% when compared to the reference case. The derivation of the optimization problem formulation was systematically checked, and error analysis was performed to assess the most probable sources of error in the solution method implemented.

Sammendrag

Hvordan termodynamiske irreversibiliteter i strømningen i ejektorer kan reduseres og hvordan optimalt design av ejektorer skal utføres er enda ikke helt forstått. Ejektorer er utstyr som brukes i forskjellige energiprosesser til å komprimere og ekspandere fluider. Bruken av numeriske strømningsberegninger og eksperimentelle studier har demonstrert at endringer i ejektorgeometrien kan påvirke ejektorens ytelse positivt. Særdeles få tidligere studier har undersøkt bruken av ikke-likevekts termodynamikk til geometrisk optimering av ejektorer. Teorien om ikke-likevekts termodynamikk kan anvendes for kvantifisering av den lokale og dermed også totale entropiproduksjonen i en prosess. Fordi energieffektive prosesser karakteriseres av lav entropiproduksjon, kan den totale entropiproduksjonen i en prosess brukes til å designe energieffektivt prosessutstyr gjennom optimering.

I denne oppgaven har entropiproduksjonen i rørstrømning blitt undersøkt, motivert av termodynamiske irreversibiliteter i strømningen i ejektorer. Arbeidshypotesen for oppgaven er at det eksisterer en optimal radius profil for et sirkulært rør, i den forstand at profilen minimerer entropiproduksjonen i strømningen. En arealmidlet éndimensjonal modell av viskøs, adiabatisk, énfase strømning av luft i et rør med varierende tverrsnitt har blitt utviklet. Ikke-likevekts termodynamikkens teori har blitt brukt for å utlede den lokale entropiproduksjonen i strømningen. Numerisk optimering og optimal kontrollteori er anvendt til optimering av radiusprofilen til rørveggen. Målet var å minimere den totale entropiproduksjonen i røret. Fluiddynamikkmodellen og optimeringsproblemene som ble formulert ble implementert på en datamskin og løst numerisk. Numerisk analyse og en termodynamisk konsistenssjekk ble gjennomført for å validere alle resultater.

Numerisk optimering resulterte i løsninger som konvergerte mot et lokalt minimum. Disse løsningene ga radiusprofiler som førte til en reduksjon på 60% av den totale entropiproduksjonen sammenliknet med et referanseoppsett. Radiusprofilenes utforming synes å være lite anvendelige for praktiske anvendelser, på grunn av negative tredimensjonale strømningseffekter som ikke er tatt høyde for i modellen i denne oppgaven. Derfor karakteriseres reduksjonspotensialet som urealistisk.

I tillegg til numerisk optimering ble optimal kontrollteori med helningen til radiusprofilen som kontrollvariabel brukt til å formulere et optimeringsproblem. Dette ble implementert og forsøkt løst iterativt uten å lykkes. Hamiltonianen som ble beregnet for et resultat gitt av den numeriske løseren brukt viste seg ikke å være konstant, noe den burde vært for problemet som var formulert. Selve fysikken for profilene løseren ga ut var konsistent med strømningsmodellen. Den resulterende radiusprofilen førte til en 45% reduksjon av den totale entropiproduksjonen sammenliknet med referanseoppsettet. Utledningen av optimeringsproblemet ble systematisk gjennomgått og feilanalyse ble gjennomført for å undersøke hva kilden til feilen i løsningsmetoden var.

Acknowledgements

The author would like to thank his supervisor Øivind Wilhelmsen for guidance and valuable support, as well as numerous interesting and helpful discussions. The co-supervisors Ailo Aasen and Krzysztof Banasiak must also be thanked for partaking in and contributing to many of the discussions. An additional thank you to the rest of the PoreLab NTNU Research Group for facilitating discussions, as well as providing both knowledge and literature on the topic of non-equilibrium thermodynamics.

Contents

Figures

Tables

Chapter 1

Introduction

The climate impact caused by humans is becoming increasingly evident. By now, there is no doubt that we must focus on limiting the causes of global warming. According to the U.S. Energy Information Administration, the industrial sector uses more delivered energy than any other end-use sector, consuming about 54% of the world's total delivered energy [1]. Enhancing the efficiency of equipment used in industrial processes is therefore paramount to aid in reducing global warming. To this end, non-equilibrium thermodynamics has proven to be a powerful and rigorous tool.

The theory of non-equilibrium thermodynamics describes transport processes in systems that are not in global equilibrium [2]. Any real process is irreversible with entropy being produced in the process. The amount of entropy produced quantifies dissipation of useful work in the process [3]. Two processes can achieve the same result, without producing the same amount of entropy. This means that one of the processes is more energy-efficient than the other.

Using efficiency metrics based on the Second Law of Thermodynamics, non-equilibrium thermodynamics provides an efficient way of analyzing energy process efficiencies [4]. For a work-demanding process requiring the work $W > 0$, the Second Law efficiency is defined as

$$\eta_{\mathrm{II}} = \frac{W_{\mathrm{ideal}}}{W},$$

where W_{ideal} is the ideal work required to accomplish the process in the absence of irreversibilities. To illustrate, consider pushing a box on a ground made of concrete. The friction forces between the box and the ground represent an irreversibility. In the absence of friction forces, pushing the box at a constant velocity would require no work to push the box around, meaning that W_{ideal} would be equal to zero. In reality, however, a work W is required to push the box around since energy is dissipated through friction. The difference between the ideal work and the real work is defined as the lost work

$$W_{\mathrm{lost}} = W - W_{\mathrm{ideal}}.$$

The lost work is the exergy that has been destroyed due to entropy production in a process. Exergy is the maximum amount of useful energy that is available in a process [5]. The lost work can also be determined with the total entropy production σ_{tot} of the process

$$W_{\mathrm{lost}} = \sigma_{\mathrm{tot}} T_0.$$

Here, T_0 is the ambient temperature. If the ideal work is fixed, minimization of the total entropy production of a process is equivalent to minimization of the lost work of a process. This is then equivalent to minimization of the work needed to accomplish the process. Quantification of the irreversibilities of a process in terms of entropy production thus provides a way of performing optimization of the process. The expressions for η_{II} and W_{lost} take on different forms when considering a work-producing

process ($W < 0$) because $|W_{\text{ideal}}| > |W|$ in that case. For work-producing processes, minimization of the entropy production for a fixed ideal work would equal maximization of the work output of the process.

Using non-equilibrium thermodynamics theory to determine the entropy production in a system is not only useful for quantifying the total lost work of the process. It also provides detailed information about exactly what parts of a process that are the sources of irreversibilities, and therefore what parts could be considered for re-design. An important, general result exists regarding the distribution of local entropy production in a process. It has been shown that for some cases, equipartitioning of entropy production is equivalent to the state of minimum entropy production [6, 7]. Equipartitioning of entropy production is equivalent to having a constant entropy production rate throughout the system. In the cases where equipartitioning of entropy production does not coincide with the state of minimum entropy production, a state of constant entropy production is at least a good approximation to the state of minimum entropy production [3, 8, 9].

Several industrial processes and their irreversibilities have previously been analyzed with non-equilibrium theory and subsequently optimized. Johannessen and Kjelstrup [10] studied a plug flow reactor and minimized the entropy production for SO_2 oxidation using optimal control theory. Entropy production due to heat exchange, viscous flow and chemical reactions were accounted for. They achieved a 10.4% reduction in the total entropy production rate when controlling the utility temperature, and an impressive 24.7% reduction when also using the length of the reactor as a varying parameter in the optimization.

Hånde and Wilhelmsen [9] studied a heat exchanger in the cryogenic part of the hydrogen liquefaction process. Optimal control theory was used to minimize entropy production, with a reduction of up to 8.7% when compared to a reference heat exchanger. They also demonstrated that equipartitioning of entropy production is indeed an excellent design principle for making energy-efficient process equipment. The amount of entropy produced in the heat exchanger for an equipartitioned state deviated less than a percent from the amount produced in the state of minimum entropy production.

The octoral hesis work of Johannessen [3] is an excellent contribution to the work on irreversible thermodynamics in process industry. He performed minimization of entropy production for several different processes using both numerical and analytical optimization techniques. Heat exchange, plug flow reactors and diabatic tray distillation were among the process equipment investigated. Reductions in the entropy production rate were achieved through optimization, using utility temperatures and chemical compositions as parameters. Results also suggested that the entropy production did not necessarily need to be equipartitioned throughout the entirety of the process when operating in an optimal state. However, certain subsections of the system often exhibit approximately equipartitioning of the entropy production.

A more recent work that is highly interesting is the nature-inspired geometrical design of a plug flow reactor done by Magnanelli *et al.* [11]. Motivated by the efficient design of the nasal geometry of reindeer, optimal control theory was used to investigate whether variations in the cross-sectional geometry of the reactor could increase its efficiency. The results showed a potential reduction of 11% of the total entropy production when varying the diameter of the reactor, and 16% when also varying the length of the reactor. These are promising results that demonstrate the power of non-equilibrium thermodynamics combined with geometric optimization.

Ejector technology is a process equipment where it is not yet fully understood how optimal and energy-efficient design of the equipment is performed. Ejectors are devices where two fluid streams at different pressures are mixed and discharged at an intermediate pressure. They are applicable in a variety of energy processes, proving useful in applications ranging from solar plants to conversion systems for ocean thermal energy [12–16]. According to Elbel and Lawrence [17], applications of ejectors in refrigeration are the most frequent, where they can be employed to recover expansion work. The use of ejectors has exhibited a potential for helping us reach the global climate goals, as

they perform well with climate-friendly refrigerants and may utilize waste-heat or extract expansion work that would otherwise have been lost in a process.

Figure 1.1 illustrates how an ejector can be used for recovery of expansion work in a refrigeration cycle, where the condenser stream is used to compress the evaporator stream before the resulting stream enters the separator. This leads to a higher pressure of the liquid entering the compressor, requiring less duty on the compressor to make the working fluid reach the desired operating conditions of the condenser. A conventional ejector geometry is illustrated in Figure 1.2.

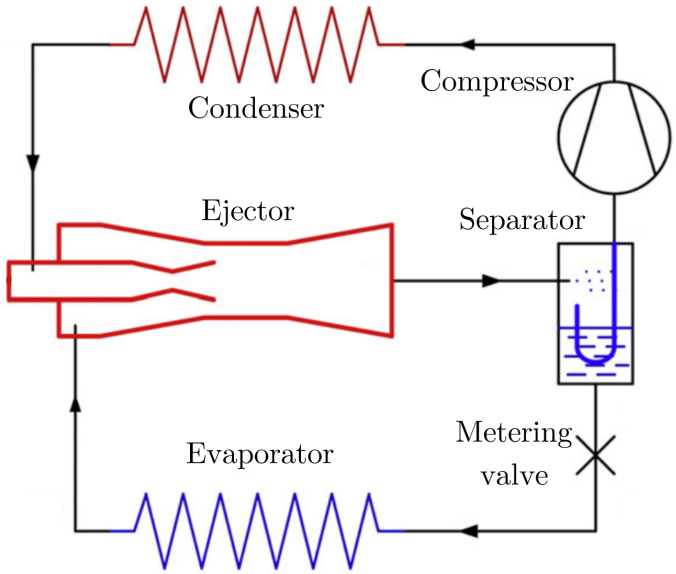

Figure 1.1: An example of the use of an ejector for recovery of expansion work in a refrigeration cycle. Adapted from [18].

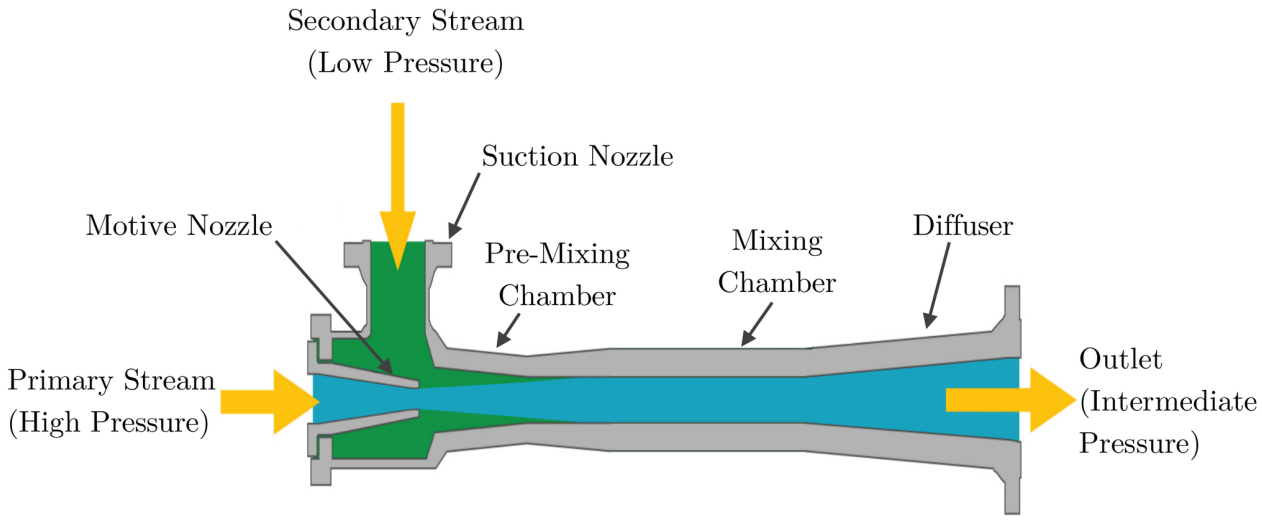

Figure 1.2: A typical ejector geometry. Two fluid streams at different pressures enter the ejector through the primary and secondary nozzles, mix, and flow downstream leaving the ejector at an intermediate pressure. Adapted from [19].

A drawback of ejectors is their low efficiency. It has been demonstrated that entropy production in ejectors is far from equipartitioned [20]. Since, as mentioned previously, equipartitioning of entropy production for some processes has proven to be either the state of minimum entropy production or a good approximation to it, this suggests that there might be room for improvement regarding design of ejectors.

Some previous works have considered thermodynamic irreversibilities in ejectors and their effect on performance [21, 22]. Results indicate that the mixing process of the two streams with resulting transfer of momentum and energy is a main source of irreversibility. The studies also showed that altering the geometry of the different pars of the ejector can have significant effects on the irreversibilities present, both their magnitude and distribution. Other works studied the effect of altering the ejector geometry to increase efficiency. For instance, Nakagawa *et al.* [23] showed that the ratio of the length and the diameter of the mixing section of two-phase ejectors is crucial for efficiency optimization.

Banasiak *et al.* [24] investigated the influence of varying geometric parameters of a two-phase CO_2 ejector used in a heat pump. The variables that were varied independently were the length and the diameter of the mixing chamber, as well as the angle of the diffuser section. They performed both experimental tests and numerical analyses. Optimal configurations for all the considered geometric variables were determined, and in general the conclusions reached were consistent with the results of earlier investigations performed by Nakagawa *et al.* [23], Elbel and Hrnjak [25], and Elbel [18]. Furthermore, both experimental and numerical results indicated significant potential for improvement of the Coefficient of Performance of the total system, not just for the ejector itself. Thus, geometric optimization of ejectors is expected to lead to positive benefits in terms of efficiency enhancement of industrial processes where they are utilized.

The flow in an ejector and its inherent thermodynamic irreversibilities serve as motivation for the present work. Inspired by earlier work on process optimization and geometrical design for efficient process equipment, we ask ourselves whether the typical ejector geometry depicted in Figure 1.2 is optimal, in the sense that it leads to minimum entropy production (given certain operating conditions). Would a curved wall profile instead of linear wall profiles in the nozzle and diffuser sections improve efficiency? Could any of the profiles illustrated in Figure 1.3 lead to better performance compared to a constant area mixing chamber? No trivial answers to these questions exist.

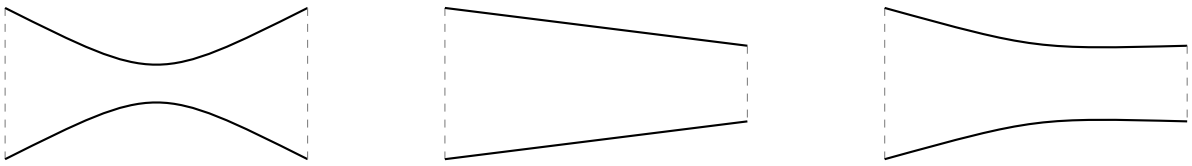

(a) Converging-Diverging **(b)** Converging (linear) **(c)** Converging (curved)

Figure 1.3: Could any of these geometries improve the performance of the constant-area mixing section of a typical ejector?

Searching for answers to these questions, the research literature does not provide a lot of guidance. Regarding geometrical optimization of devices with confined flows, Sahin [26] performed an interesting study to find the optimal cross-sectional shape of a constant area pipe for minimization of entropy production of the flow. Consistent with intuition, the resulting profile was circular. Some other previous research exists which covers the irreversibilities of confined viscous flow [27–30], but the amount of research literature covering entropy production minimization in confined flows is scarce. To the best of this author's knowledge, no work has yet been done on optimization by minimization of entropy production for viscous flow in confined geometries using variations in the radius or wall profile as the optimization parameter. This is rather peculiar, considering the importance of confined flows in engineering practice. Oil and gas pipe flow, air ducts, nozzles, and diffusers used in process

equipment – the applications are numerous.

As a very first step to assess the optimality of the ejector geometry, a model of fluid flow through a pipe of varying cross section was established and analyzed in the present work. The thermodynamic irreversibilities of the flow were quantified. The model together with a framework for optimization was implemented in MATLAB, with all the code being original except for a few built-in functions. Numerical optimization and optimal control theory were used to perform optimization of the radius profile of the pipe, with minimization of the entropy production as the goal of the optimization. Hopefully, this work can spark further interest in analysis of entropy production in viscous flows. The ultimate goal is to be able to provide some guidelines for efficient profile design of pipe geometries, or at least facilitate further research on the topic.

Chapter 2

Theory

In this chapter, governing equations of the flow that will be analyzed are derived in the first section. Next follows a section covering general theory of irreversible thermodynamics as well as analysis of the irreversibilities of the current problem. Mathematical optimization is covered in the last section of the chapter, where the two optimization methods used in this work are introduced. Constrained optimization is covered first. Then follows a brief introduction to optimal control theory, as well as the optimal control theory problem formulation for the present work.

2.1 Fluid Dynamics in a Pipe of Variable Cross-Sectional Area

To approximate the flow in some parts of an ejector, we will consider flow of a single-phase fluid in a pipe of length L with cross-sectional area A. The area varies as a function of the axial coordinate z as illustrated in Figure 2.1. The cross section is circular, such that $A = \pi r^2$, with the radius r being a function of z.

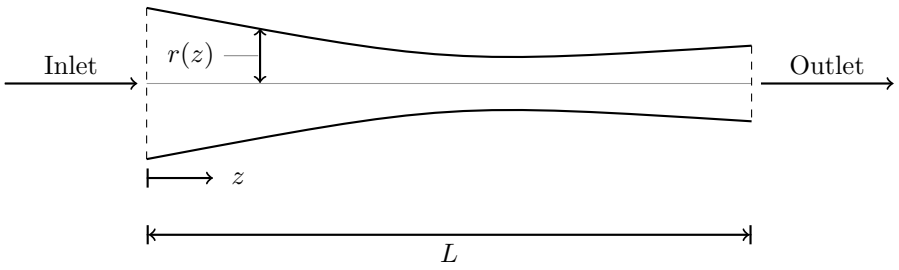

Figure 2.1: Single-phase fluid flow enters at the left-hand side and flows through a pipe with variable cross-sectional area. The pipe length is L and the axial coordinate is z, which the radius of the cross section $r(z)$ is a function of.

We will consider a one-dimensional model where the density ρ, velocity V, pressure P and temperature T of the fluid are all assumed to only have a component in the z direction. The variables are then effectively averaged over the cross section. This approach, a so-called plug flow formalism, leads to no knowledge of the lateral distribution of the flow variables [31]. Two- and three-dimensional flow features are thus not fully accounted for. In turn it greatly simplifies the mathematics of the problem. Despite of their simplicity, such one-dimensional models can yield valuable insight of the flow mechanisms, but their limitations should be respected [32].

Furthermore, the flow is assumed to be at steady state, meaning that the variables are constant with respect to time. The fluid is modeled as single-phase air behaving as an ideal gas. It is further assumed that the flow is adiabatic, with no heat transferred to the fluid through the pipe wall.

At steady state, the mass flow rate $\dot{m} = \rho AV$ in the pipe is constant. Differentiation with respect to z therefore yields

$$\frac{d(\rho AV)}{dz} = 0 \tag{2.1}$$

or alternatively

$$\frac{1}{\rho}\frac{d\rho}{dz} + \frac{1}{A}\frac{dA}{dz} + \frac{1}{V}\frac{dV}{dz} = 0.$$

With the above introduced assumptions and additionally neglecting effects of gravity due to the height of the pipe above the ground being constant, the momentum equation of the flow reads

$$\frac{d(A\rho V^2)}{dz} + A\frac{dP}{dz} = -\frac{f\rho V^2}{8}\frac{dS}{dz} \tag{2.2}$$

where the term on the right-hand side is the steady-state approximation of the wall shear stress [31]. In Equation (2.2), dS/dz is the local local change in surface area or equivalently the local perimeter of the cross section, and f is the Fanning friction factor. In general, the friction factor is a function of wall roughness, pipe diameter and the Reynolds number of the flow. The Reynolds number dependency weakens as the flow becomes increasingly turbulent, reaching a regime where the friction factor is approximately constant. Here we will assume that the flow is in this regime, which is mostly the case for ejector flow.

Next, the energy equation is established. Changes in potential energy are neglected because the effects of gravity are neglected. Together with the assumptions of the flow being steady-state and adiabatic, the energy equation reads

$$\frac{d(\rho AV\,(h + V^2/2))}{dz} = 0 \tag{2.3}$$

where h is the specific enthalpy of the fluid. Using the continuity equation (2.1), we can simplify Equation (2.3) to

$$\frac{d(h + V^2/2)}{dz} = \frac{dh}{dz} + V\frac{dV}{dz} = 0, \tag{2.4}$$

which is equivalent to stating that the stagnation enthalpy $h_s = h + V^2/2$ is constant. As mentioned previously, the fluid in this work is air modeled as an ideal gas. An ideal gas is assumed to consist of point particles not subjected to interparticle interactions. Therefore, internal energy and also the specific enthalpy h of the gas is only a function of its temperature [33]. Infinitesimal changes in h and T are related through $dh = c_p dT$, where c_p is the specific heat capacity of the gas at constant pressure [5]. With this, Equation (2.4) takes the form

$$c_p\frac{dT}{dz} + V\frac{dV}{dz} = 0. \tag{2.5}$$

The last governing equation is the thermodynamic equation of state. For an ideal gas, this equation of state relates the pressure, density and temperature through

$$P = \rho RT \tag{2.6}$$

were R is the specific gas constant in units of J/kgK. Alternatively, the equation can be formulated on differential form:

$$\frac{1}{P}\frac{dP}{dz} = \frac{1}{\rho}\frac{d\rho}{dz} + \frac{1}{T}\frac{dT}{dz}. \tag{2.7}$$

We now have four equations at hand to solve for the four variables ρ, V, P, T. The area A, or more specifically the radius r, is also a variable in the governing equations, leaving us with four equations

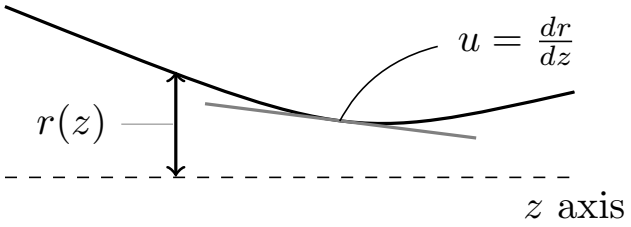

Figure 2.2: The slope u of the radius is defined as the slope of the tangent of $r(z)$ at an axial coordinate z.

to solve for five unknowns. Assume for the time being that the slope of the radius of the cross section at a given z coordinate, denoted u, is pre-determined. See Figure 2.2 for an illustration. We could then determine the radius of the cross section by integration of the differential equation

$$\frac{dr}{dz} = u. \tag{2.8}$$

Normally, the flow variable profiles in the pipe would now be determined by integration of the governing equations (2.1), (2.2), (2.5), (2.7) and (2.8). In this work, a different approach is taken to reduce the number of ordinary differential equations (ODEs) needed to be solved. Since we can solve the algebraic equations exactly without the need for integration, this is advantageous because it reduces computational cost and numerical inaccuracy when implementing the problem on a computer and solving it numerically.

If we take the momentum equation

$$\frac{d(A\rho V^2)}{dz} + A\frac{dP}{dz} = -\frac{f\rho V^2}{8}\frac{dS}{dz}$$

and rewrite the pressure derivative by using the product rule

$$\frac{d(PA)}{dz} = P\frac{dA}{dz} + A\frac{dP}{dz},$$

we get

$$\frac{d(A\rho V^2)}{dz} + \frac{d(PA)}{dz} - P\frac{dA}{dz} = \frac{d\left(A\left(P+\rho V^2\right)\right)}{dz} - P\frac{dA}{dz} = -\frac{f\rho V^2}{8}\frac{dS}{dz}. \tag{2.9}$$

Defining the momentum flow rate $\dot{M} = A(P + \rho V^2)$ and rearranging terms in Equation (2.9) yields

$$\frac{d\left(A\left(P+\rho V^2\right)\right)}{dz} = \frac{d\dot{M}}{dz} = P\frac{dA}{dz} - \frac{f\rho V^2}{8}\frac{dS}{dz}. \tag{2.10}$$

With a set of inlet conditions for $\dot{M}$ and r at the inlet of the pipe, we can determine r and $\dot{M}$ for a given u profile by integration of Equation (2.8) and Equation (2.10) over the pipe length, since this constitutes an initial value problem. The variables ρ, V, P, T can then be solved for using the algebraic relations

$$\dot{m} = \rho A V \tag{2.11}$$

$$h_s = c_p\left(T - T_{\text{ref}}\right) + V^2/2 \tag{2.12}$$

$$P = \rho R T \tag{2.13}$$

$$\dot{M} = A\left(P + \rho V^2\right) \tag{2.14}$$

with T_{ref} being the reference temperature for enthalpy calculations. This reference temperature is needed because enthalpy is a state function. A reference enthalpy is set at a reference temperature,

and then enthalpies are calculated with respect to the reference enthalpy [5]. In physical systems with several chemical components, one needs to set the reference enthalpy based on enthalpies of formation at a reference temperature to ensure correctness in the calculations. For a single-component gas as considered in this work, however, the choice of reference can be arbitrary.

2.2 Irreversible Thermodynamics

Important theory of non-equiblirium thermodynamics mentioned in the introduction is covered more in detail in this section. One subsection is dedicated to the derivation of the local entropy production in the pipe flow model developed in the previous section. An expression for the entropy difference between two states for an ideal gas is also introduced.

2.2.1 Lost Work, Entropy Production and Process Efficiency

Some applications of non-equiblirium thermodynamics were discussed in Chapter 1, as well as results showing the usefulness of the theory in optimization of energy efficiency. It was stated that minimization of entropy production is equivalent to minimization of lost work in a process, if the ideal work of the process is fixed. This is demonstrated here more theoretically. The theory covered in the following is based on the material in Kjelstrup *et al.* [2] and Bejan [4]. See these references for more details. The theory outlined will be used as motivation for the optimization work in this thesis, which is discussed at the end of the subsection.

The classical formulation of the Second Law of Thermodynamics states that, for a process, the total entropy change

$$\Delta s + \Delta s_0 \geq 0,$$

where Δs is the change in specific entropy of the process materials and Δs_0 is the specific entropy change of the environment. In words, the entropy of the closed system that confines the process may never decrease. For a reversible process, the total entropy change of the system would be zero. For an irreversible process, define the average total entropy production rate $\dot{\sigma}_{\text{tot}}$ in the time interval Δt. The total entropy production in the process is then

$$\sigma_{\text{tot}} = \dot{\sigma}_{\text{tot}} \Delta t = \Delta s + \Delta s_0. \tag{2.15}$$

Let us consider here a work-demanding process. The minimum amount of work input needed to accomplish the process would be the reversible case, i.e. $\sigma_{\text{tot}} = 0$. Denote this work W_{ideal}. Because of irreversibilities, a real work W which is greater than W_{ideal} is required to accomplish the process, and the difference between the two is defined as the lost work

$$W_{\text{lost}} = W - W_{\text{ideal}} = T_0 \dot{\sigma}_{\text{tot}} \Delta t, \tag{2.16}$$

which is also known as the Gouy-Stodola theorem [4]. In Equation (2.16), T_0 is the ambient temperature. The right-hand side of the equations is also sometimes referred to as exergy destruction, because it represents the amount of exergy (useful energy) that is destroyed in a process due to irreversibilities.

With the theory of non-equiblirium thermodynamics, we can calculate the total entropy change of a system by integrating the local entropy production over the volume of the system

$$\sigma_{\text{tot}} = \int_V \sigma_V dV \tag{2.17}$$

and then multiplying with the ambient temperature we get the lost work

$$W_{\text{lost}} = T_0 \sigma_{\text{tot}} = T_0 \int_V \sigma_V dV. \tag{2.18}$$

We thus have two ways of calculating the lost work of the process. Either by determining the total entropy change $\Delta s + \Delta s_0$, or by integration of the local entropy production σ_V. Knowledge of the local entropy production can give us detailed information of where work is lost in a process, whereas the entropy balance over the system is a macroscopic approach. Since the two expressions (2.15) and (2.17) should be equal, quantifying the total entropy change of the system in both ways can serve as a consistency check of our model of a system. Owing to Equation (2.18), minimization of the lost work equals minimization of entropy production if the ideal work of the process is fixed. This shows that a process with minimum entropy production is an energy-efficient process.

Because the pipe flow model developed here is motivated by flow in ejectors, this work will regard the last section of the ejector which is the diffuser section. The main purpose of an ejector diffuser section is to increase the pressure of the working fluid. With the inlet conditions given, we could quantify the efficiency of the process by the outlet pressure, which is what we want to maximize. The maximum expansion work that can be performed in the flow process would be in the case of an isentropic flow where no entropy was produced. This would correspond to the ideal work of the flow process.

Because of entropy production, we cannot extract the ideal expansion work from the process, but minimization of the entropy production could lead us closer to the ideal work since less entropy production would mean less lost work. For example, for a set of inlet conditions and with the pipe outlet radius set, it would be interesting to investigate whether minimization of the entropy production in the pipe would lead to maximization of the outlet pressure. Intuitively, this could be the case because the pipe flow model accounts for friction forces, which are directly related to viscous dissipation and thus loss of momentum. The local entropy production derived in the next subsection will elucidate this relationship. Another interesting case to investigate would be setting the outlet pressure to a given value, but leaving the radius at the outlet a free variable. This could lead to maximization of the outlet velocity when the total entropy production is minimized, as entropy production minimization would represent finding the most efficient way of reaching the outlet pressure given the flow state at the inlet of the pipe. However, detailed analysis of the relationship between pressure change, velocity change and entropy production is required to answer these questions. This is the focus of the optimization work in this thesis.

2.2.2 Pipe Flow Irreversibilities

To analyze in detail the irreversibilities of the pipe flow model introduced in Section 2.1, we need an explicit expression for the local entropy production σ. To derive this expression, let us consider an infinitesimal control volume of cross-sectional area A and width dz. The volume can then be approximated as $dV = Adz$, since both dz and the changes in A are infinitesimal. See Figure 2.3. The fluid flowing through the control volume experiences an infinitesimal change ds in its specific entropy s. At steady state, the accumulation of entropy within the control volume over time is equal to zero. With the assumption of adiabatic flow, the net change in the entropy convected with the flow must then equal the total entropy production in the control volume:

$$\sigma_V dV = \dot{m}((s + ds) - s) = \dot{m}ds. \tag{2.19}$$

Here, σ_V is the volumetric entropy production and has units of $\mathrm{W/m^3K}$.

Using the developments of Section 2.1, the momentum equation and the energy equation of the flow, respectively, read

$$\frac{d(A\rho V^2)}{dz} + A\frac{dP}{dz} = -\frac{f\rho V^2}{8}\frac{dS}{dz}, \tag{2.20}$$

$$\frac{dh}{dz} + V\frac{dV}{dz} = 0. \tag{2.21}$$

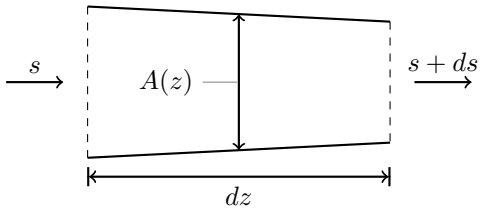

Figure 2.3: A control volume of width dz and cross-sectional area $A(z)$, and thus infinitesimal volume $dV = Adz$. The flow enters at the left-hand side at z with specific entropy s, and exits the control volume at $z + dz$, experiencing a change ds in the entropy.

Using the assumption of steady state, we have

$$\frac{d(A\rho V^2)}{dz} = \frac{d(\rho AV)}{dz} + \rho AV\frac{dV}{dz} = \rho AV\frac{dV}{dz}$$

owing to the continuity equation, so Equation (2.20) can be rewritten as

$$\frac{dP}{dz} = -\rho V\frac{dV}{dz} - \frac{f\rho V^2}{8A}\frac{dS}{dz}. \tag{2.22}$$

Now, envoking Gibbs' relation

$$T\frac{ds}{dz} = \frac{dh}{dz} - v\frac{dP}{dz}$$

where $v = 1/\rho$ is the specific volume [5], and inserting expressions for dh/dz and dP/dz from Equation (2.21) and Equation (2.22), we get

$$\begin{aligned} T\frac{ds}{dz} &= \frac{dh}{dz} - \frac{1}{\rho}\frac{dP}{dz} \\ &= -V\frac{dV}{dz} - \frac{1}{\rho}\left(-\rho V\frac{dV}{dz} - \frac{\rho V^2 f}{8A}\frac{dS}{dz}\right) \\ &= \frac{V^2 f}{8A}\frac{dS}{dz}. \end{aligned} \tag{2.23}$$

Together with Equation (2.19) this results in

$$\sigma = A\sigma_V = \dot{m}\frac{ds}{dz} = \frac{\dot{m}}{T}\frac{V^2 f}{8A}\frac{dS}{dz} \tag{2.24}$$

where σ is the local entropy production per unit length. It is evident that the only contribution to entropy production in the flow given the current assumptions is that due to viscous dissipation through the wall friction forces. We also see from Equation (2.23) that the advection term VdV/dz vanishes from the entropy change expression, indicating that this term pertains to reversible momentum transfer.

Two geometrical properties appear in the local entropy production expression. For a circular cross section, the cross-sectional area $A = \pi r^2$, where r is the radius. The differential change in local surface area dS/dz of the pipe, can be derived with the aid of Figure 2.4. Since the cross section is circular at every axial coordinate, the infinitesimal surface area dS of a part of the pipe at a position z can be found by revolution about the z axis of a small band of width ds and height $r(z)$. The width ds is the arc length of the arc connecting the peripheries of two circular slices positioned dz apart from each other along the z axis. The infinitesimal difference between the radii of the slices is dr.

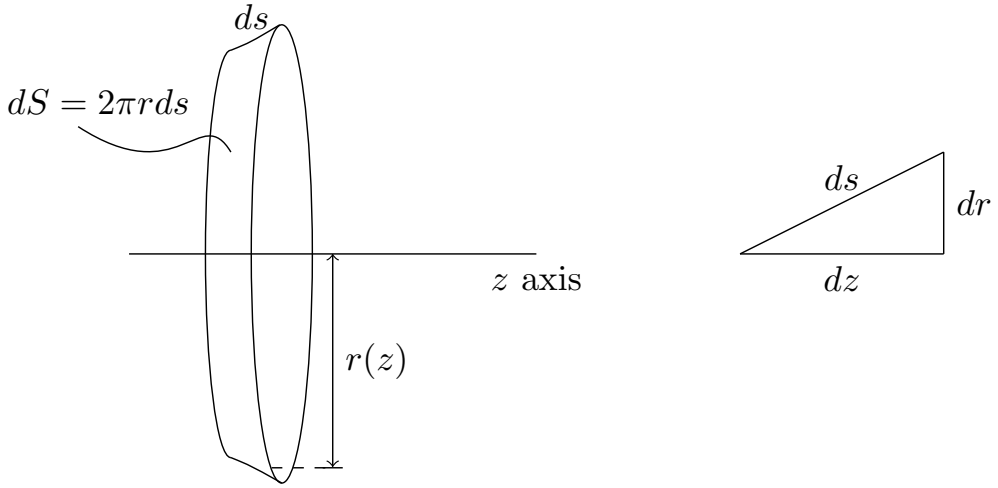

Figure 2.4: Left: An infinitesimal surface area element of the pipe, created by taking a band of width ds and height $r(z)$ and revolving it about the z axis, resulting in the infinitesimal surface area dS. **Right:** If the arc ds is infinitesimally short, its length can be approximated with the Pythagorean theorem, where the catheti of the triangle are the distance dz between the slices enclosing the band and the difference dr of their radii.

Assuming ds to be infinitely short, its length is given by $ds = \sqrt{dz^2 + dr^2}$. The surface area dS of the band can now be found by multiplying ds with the perimeter of the slice

$$dS = 2\pi r\sqrt{dz^2 + dr^2} = 2\pi r\sqrt{1 + \left(\frac{dr}{dz}\right)^2}\,dz$$

where dz has been factored out of the square root so that we can solve for the surface area differential:

$$\frac{dS}{dz} = 2\pi r\sqrt{1 + \left(\frac{dr}{dz}\right)^2}.$$

The resulting expression for the local entropy production in a pipe with circular cross section is then

$$\sigma = \frac{\dot{m}}{T}\frac{V^2 f}{8A}\frac{dS}{dz} = \frac{\dot{m} f}{4}\frac{V^2}{rT}\sqrt{1 + \left(\frac{dr}{dz}\right)^2}. \tag{2.25}$$

The total entropy production in the pipe is equal to the integral of the local entropy production over the entire pipe length

$$\sigma_{\text{tot}} = \int_0^L \sigma dz = \int_0^L \frac{\dot{m} f}{4}\frac{V^2}{rT}\sqrt{1 + \left(\frac{dr}{dz}\right)^2}\,dz. \tag{2.26}$$

2.2.3 Entropy Change of an Ideal Gas

The calculation of the difference in entropy between two thermodynamic states of the fluid will prove useful in this work. It will prove valuable insight when discussing the irreversibilities of the flow process, and can as mentioned earlier be used for a thermodynamic consistency check.

For an ideal gas, the local Gibbs' relation $Tds = dh - vdP$ can be altered by envoking the relation $Pv = RT$, such that

$$ds = \frac{dh}{T} - \frac{v}{T}dP = \frac{dh}{T} - R\frac{dP}{P}. \tag{2.27}$$

During derivation of the pipe flow model in Section 2.1, the change in enthalpy for an ideal gas was introduced: $dh = c_p dT$. Inserted into Equation (2.27) this yields

$$ds = c_p \frac{dT}{T} - R\frac{dP}{P}. \tag{2.28}$$

Assuming a constant specific heat capacity c_p and integrating Equation (2.28) from state 1 to state 2 gives the entropy difference between the two states:

$$\begin{aligned} \int_1^2 ds = s_2 - s_1 &= c_p \int_1^2 \frac{dT}{T} - R\int_1^2 \frac{dP}{P} \\ &= c_p \ln\frac{T_2}{T_1} - R\ln\frac{P_2}{P_1}. \end{aligned} \tag{2.29}$$

2.2.4 Entropy Differences and Total Entropy Production

With the expressions derived in Section 2.2.2 and Section 2.2.3, we now have two ways of calculating the total entropy change in the pipe flow modeled. We can either determine the total entropy production by integration (Equation (2.26)) or calculate the entropy difference using Equation (2.29), by setting state 1 to the inlet state at $z_0 = 0$ and state 2 to the outlet state at $z_f = L$. These two calculations must be equal, meaning that

$$\sigma_{\text{tot}} = \dot{m}\int_{z=0}^{z=L} ds = \dot{m}(s_f - s_0) = \dot{m}\int_{z=0}^{z=L} c_p\frac{dT}{T} - R\frac{dP}{P}. \tag{2.30}$$

where $\dot{m}$ could be taken outside the first integral since the flow is assumed to be at steady state. Subscript 0 refers values at the pipe inlet, whereas subscript f refers to outlet values. Using the energy balance

$$c_p dT + V dV = c_p dT + d\left(\frac{V^2}{2}\right) = 0$$

in Equation (2.30) we get

$$\frac{\sigma_{\text{tot}}}{\dot{m}} = \int_{z=0}^{z=L} \frac{-d(\frac{V^2}{2})}{T} - R\frac{dP}{P}. \tag{2.31}$$

The pressure integral is of the form

$$\int_{z=0}^{z=L} \frac{dx}{x} = \int_{z=0}^{z=L} d(\ln x) = \ln\left(\frac{x_f}{x_0}\right)$$

such that

$$\frac{\sigma_{\text{tot}}}{\dot{m}} = -R\ln\frac{P_f}{P_0} - \int_{z=0}^{z=L} \frac{d(\frac{V^2}{2})}{T}, \tag{2.32}$$

where P_f is the final pressure at the outlet of the pipe and P_0 is the inlet pressure. Equation (2.32) demonstrates that minimizing the entropy production and maximizing the pressure lift P_f/P_0 is not fully equivalent, because we have a third term in the equation, the integral on the right-hand side, that in a way quantifies the kinetic energy change in the pipe. Had we postponed the integration a little bit, we would in fact for a frictionless flow with $\sigma = 0$ and using the ideal gas relation $P = \rho RT$ recover the compressible Bernoulli equation from Equation (2.32). The Bernoulli equation relates pressure changes to changes in kinetic energy through proportionality in the reversible case [34]. In an irreversible flow, we cannot achieve the same kinetic energy change for a given pressure change because of the entropy production (or vice versa). Note that Equation (2.32) implicitly puts a bound on the pressure and velocity changes, because the Second Law of Thermodynamics requires that $\sigma_{\text{tot}} \geq 0$.

2.3 Optimization

With a fluid dynamic model of the pipe flow developed and with an expression for the total entropy production in the pipe derived, we will now turn to the theory of the optimization done in this work.

First, constrained optimization will be covered. This approach maximizes or minimizes a scalar objective function given problem-specific constraints. Optimization is then based on finding a set of variables that optimizes the objective function. The numerical solution to this problem can then be found with mathematical programming.

Second, a brief introduction to optimal control theory is given. A control variable is chosen as the controllable input of a system, and an optimal way of controlling the system is determined. Optimal control theory is a mathematical theory based on calculus of variations, and deals with optimization of functionals (functions of functions). The functional in this work will be the integral of a function. The solution space is then a set of functions. After the brief introduction to optimal control theory, the problem formulation for the present work is handled.

The reason why these two optimization methods were chosen was that the first one (constrained optimization) was considered rather simple to formulate a problem for and implement on the computer, potentially leading to an early establishment of what types of solutions to the optimal pipe radius profile problem we can expect to find. The second approach (optimal control theory) is more elaborate than the first, but is considered a more suitable approach for the current problem. This is because it deals with finding functions that minimize a functional, and a function for the radius is exactly the goal of the optimization.

2.3.1 Constrained Optimization

Constrained optimization deals with problems where the goal is to maximize or minimize an objective function $f(x_i)$ of n variables $x_i \in \mathbb{R}^n$, with the variables subject to certain constraints [35]. Different types of constraints exist, but in this work we will only deal with equality constraints on the variables which can be written as functions on the form $c_j(x_i) = 0$, given a problem with j number of constraints. A minimization problem can be defined as

$$\min_{x_i} f(x_i)$$
$$\text{subject to } c_j(x_i) = 0,$$

that is, we want to find the variables x_i that minimize the function f while the constraints $c_j(x_i)$ are satisfied. In this work, we seek to minimize the entropy production of the flow. A natural choice for the objective function is then the total entropy production in the pipe, which was determined in Section 2.2.2:

$$\sigma_{\text{tot}} = \int_0^L \sigma dz = \int_0^L \frac{\dot{m} f}{4} \frac{V^2}{rT} \sqrt{1 + \left(\frac{dr}{dz}\right)^2} dz.$$

Our objective function is a function of the variables $x_i = [\rho \ V \ P \ T \ r \ u]^{\text{T}}$ with $u = dr/dz$. These variables are constrained by the governing equations of the flow as well as the boundary conditions

at the inlet and outlet of the pipe. We can thus formulate the optimization problem as

$$\begin{aligned} &\min_{x_i} \sigma_{\text{tot}} \\ &\text{subject to} \\ &\frac{1}{\rho}\frac{d\rho}{dz} + \frac{1}{A}\frac{dA}{dz} + \frac{1}{V}\frac{dV}{dz} = 0 \\ &\frac{d\dot{M}}{dz} - P\frac{dA}{dz} + \frac{f\rho V^2}{8}\frac{dS}{dz} = 0 \\ &c_p\frac{dT}{dz} + V\frac{dV}{dz} = 0 \\ &\frac{1}{P}\frac{dP}{dz} - \frac{1}{\rho}\frac{d\rho}{dz} - \frac{1}{T}\frac{dT}{dz} = 0. \end{aligned} \tag{2.33}$$

Thus, we want to find the variables x_i that minimize the total entropy production whilst satisfying the governing equations of the flow. Note that all of the governing equations were formulated on differential form when used as constraints, because using the algebraic forms lead to stability problems with the numerical solution.

In addition to the governing equations, the boundary conditions imposed on the flow serve as equality constraints. For example, if a variable x_i is specified to be equal to the value ξ at the inlet of the pipe, one would use

$$x_i(z = 0) - \xi = 0 \tag{2.34}$$

as an equality constraint. A total of six boundary conditions will be imposed on the flow in this work. The specific boundary conditions used in the optimization are outlined in Chapter 3.

The problem defined by Equation (2.33) together with Equation (2.34) consists of minimizing a function of six variables, subject to ten constraints. The number of dimensions of the problem is sizeable, and the problem may therefore potentially have several solutions. The algorithm used in the present work finds solutions that satisfy first-order criteria necessary for optimality. These are based on the gradient of the objective function, and a point is characterized as a solution if the gradient metric is equal to zero (within a certain numerical tolerance). A solution is then a local minimum or a saddle point. The point then needs to be characterized by the Hessian matrix of the objective function, which is a matrix who's entries are the second partial derivatives of the objective function with respect to its variables. Moreover, to be able to ensure that a minimum is a global minimum, the function would have to be convex in its entire domain [35]. The convexity of the objective function can be determined with its Hessian matrix. Since establishment of the Hessian here would require the calculation of 36 partial derivatives, this was not prioritized in this work.

2.3.2 A Brief Introduction to Optimal Control Theory

General theory and the most important results of optimal control theory are outlined in this subsection. The brief introduction provided draws upon the material found in Liberzon [36] and Bryson and Ho [37].

Consider a physical system with state variables x_i that depend on the spatial coordinate z. The state variables are governed by the state equations

$$\frac{dx_i}{dz} = f_i(z, x_i). \tag{2.35}$$

In optimal control theory, we choose a number of the system variables to be our control variables u_j. These will be our handles on the system, which we can use to control the state of the system at any

spatial position. Slightly adjusting the notation of Equation (2.35) we have now instead

$$\frac{dx_i}{dz} = f_i(z, x_i, u_j). \tag{2.36}$$

Let us now define a performance index, or cost-functional, for our optimization problem:

$$\mathcal{L}(z, x_i, u_j) = \int_{z_0}^{z_f} L(z, x_i, u_j) dz. \tag{2.37}$$

Here, $L(z, x_i, u_j)$ is the performance index or local cost at a given position in a given state of the system, and z_0 and z_f denote the initial and final positions. It has proven to be convenient to now define the Hamiltonian, a function central to optimal control theory, as

$$\mathcal{H} = L(z, x_i, u_j) + \lambda_i(z) f_i(z, x_i, u_j), \tag{2.38}$$

where λ_i are so-called costate variables or multiplier functions. Einstein summation convention is applied in Equation (2.38), meaning that multiple indices imply summation over that index.

The Hamiltonian can be used to derive all the necessary conditions for an optimal trajectory – the choice of control variables that maximize or minimize the cost-functional. For a problem of arbitrary dimensionality, we have

$$x_i = \begin{bmatrix} x_1 \\ x_2 \\ \vdots \\ x_{n-1} \\ x_n \end{bmatrix} = \text{state variables}, \qquad u_j = \begin{bmatrix} u_1 \\ u_2 \\ \vdots \\ u_{m-1} \\ u_m \end{bmatrix} = \text{control variables},$$

$$f_i = \begin{bmatrix} f_1 \\ f_2 \\ \vdots \\ f_{n-1} \\ f_n \end{bmatrix} = \text{system dynamics}, \qquad \lambda_i = \begin{bmatrix} \lambda_1 \\ \lambda_2 \\ \vdots \\ \lambda_{n-1} \\ \lambda_n \end{bmatrix} = \text{multiplier functions}.$$

Our goal is now to minimize the cost-functional $\mathcal{L}$, given the constraints of the system dynamics f_i. The necessary conditions for finding the optimal controls u_j to achieve this are

$$\frac{\partial \mathcal{H}}{\partial u_j} = 0, \tag{2.39}$$

$$\frac{\partial \mathcal{H}}{\partial x_i} = -\frac{d\lambda_i}{dz}, \tag{2.40}$$

$$\frac{\partial \mathcal{H}}{\partial \lambda_i} = \frac{dx_i}{dz}, \tag{2.41}$$

for all i, j [37]. The first set of conditions (2.39) are algebraic equations. The conditions (2.40) are differential equations that describe how the multiplier functions λ_i evolve in space. The conditions (2.41) simply reduce to (2.36), namely the equations governing the system dynamics.

The conditions (2.40) and (2.41) are differential equations that, with boundary conditions, constitute a two-point boundary value problem (BVP). Solution existence and uniqueness to complicated BVP are not necessarily satisfied. The BVP may have none, exactly one, or infinitely many solutions [38]. Solutions to optimal control theory minimization problems can be characterized as minima or saddle points by calculation of the second order variations of the Hamiltonian, analogous to the way of characterizing minimization solutions through calculation of the Hessian matrix for constrained

optimization. Calculations of the second order variations of the Hamiltonian were not prioritized here, as the main focus in this work was on formulating the problem and obtaining a solution.

As previously mentioned, there is an important difference between the optimization methods introduced in this and the previous subsection, constrained optimization and optimal control theory. The first method deals with optimization of a scalar function, which is a function of a vector of variables, and we search for the variables that optimize the function. In optimal control theory, we are looking for the functions that optimize the performance index which is a functional (in this case an integral). This is done by performing small variations in the input functions, in the search for the set of functions that optimize the cost-functional.

Therefore, the two methods lead to different solution procedures for the problem formulations in the present work when implemented on a computer and solver numerically. In constrained minimization, a first-order optimality measure based on the gradient of the objective function is used to iterate towards a point of lower objective function value. The solver converges towards a point where the combination of variables lead to a low objective function value, without violating the constraints of the problem. In optimal control theory, the necessary conditions Equations (2.39)–(2.41) for a minimum lead to a boundary value problem which, when solved, yields a set of functions that constitute a state where the Hamiltonian is stationary. These functions then either minimize the cost-functional or is a saddle point. The necessary conditions imply that any arbitrary perturbation in the resulting functions would lead to a higher value of the performance index (at least locally). This makes optimal control theory apt for the current problem formulation, since a function for the radius profile is precisely the goal of the optimization problem formulated.

2.3.3 Optimal Control Theory to Minimize Entropy Production in Pipe Flow

In this work, the goal is to minimize the total entropy production of the pipe flow modeled as outlined in Section 2.1. The slope of the radius of the cross section, defined as $u = dr/dz$, is chosen to be the control variable. With the expressions for entropy production derived in Section 2.2.2, the cost-functional is the total entropy production

$$\sigma_{\text{tot}} = \int_0^L \sigma dz = \int_0^L \frac{\dot{m} f}{4} \frac{V^2}{rT} \sqrt{1+u^2} dz, \tag{2.42}$$

The state variables are the momentum flow rate $\dot{M}$ and the radius r, with $\dot{M}$ depending on the flow variables ρ, V, P and T. The equations governing the state variables, Equation (2.10) and Equation (2.8), expressed in terms of the flow variables and the control variable u read

$$\frac{d\dot{M}}{dz} = 2\pi r P u - \frac{\pi r f \rho V^2}{4} \sqrt{1+u^2}, \tag{2.43}$$

$$\frac{dr}{dz} = u. \tag{2.44}$$

The Hamiltonian of the problem thus takes the form

$$\begin{aligned} \mathcal{H} &= \sigma + \lambda_1 \frac{d\dot{M}}{dz} + \lambda_2 \frac{dr}{dz} \\ &= \frac{\dot{m} f V^2}{4rT} \sqrt{1+u^2} + \lambda_1 \left(2\pi r P u - \frac{\pi r f \rho V^2}{4} \sqrt{1+u^2} \right) + \lambda_2 u \end{aligned} \tag{2.45}$$

The necessary conditions for a minimum (Equations (2.39)–(2.41)) become

$$\frac{\partial \mathcal{H}}{\partial u} = 0, \tag{2.46}$$

$$\frac{\partial \mathcal{H}}{\partial \dot{M}} = -\frac{d\lambda_1}{dz}, \tag{2.47}$$

$$\frac{\partial \mathcal{H}}{\partial r} = -\frac{d\lambda_2}{dz}, \tag{2.48}$$

$$\frac{\partial \mathcal{H}}{\partial \lambda_1} = \frac{d\dot{M}}{dz}, \tag{2.49}$$

$$\frac{\partial \mathcal{H}}{\partial \lambda_2} = \frac{dr}{dz}. \tag{2.50}$$

Equation (2.46) is an algebraic equation, whereas Equations (2.47)–(2.50) are differential equations. To solve the latter, four boundary conditions are needed. If a state variable is specified at an endpoint of the domain, its respective multiplier function is unspecified at that endpoint. If a state variable is unspecified at an endpoint of the domain, the value of the respective multiplier function at that endpoint follows from the so-called transversality condition [37].

Carrying out the partial differentiation in Equation (2.46) of the Hamiltonian with respect to u, holding the variables constant, we get

$$\frac{\partial \mathcal{H}}{\partial u} = \frac{\dot{m} f V^2}{4rT} \frac{u}{\sqrt{1+u^2}} + \lambda_1 \left(2\pi r P - \frac{\dot{m} f V}{4r} \frac{u}{\sqrt{1+u^2}} \right) + \lambda_2 = 0 \tag{2.51}$$

where the second term in the governing equation of the momentum flow rate has been slightly altered by using $\pi r \rho V = \dot{m}/r$. Equation (2.51) can be solved for λ_2 to yield

$$\lambda_2 = \lambda_1 \left(\frac{\dot{m} f V}{4r} \frac{u}{\sqrt{1+u^2}} - 2\pi r P \right) - \frac{\dot{m} f V^2}{4rT} \frac{u}{\sqrt{1+u^2}}. \tag{2.52}$$

Inserting this expression into the Hamiltonian (Equation (2.45)), we get

$$\begin{aligned} \mathcal{H} = {} & \frac{\dot{m} f V^2}{4rT} \sqrt{1+u^2} + \lambda_1 \left(2\pi r P u - \frac{\dot{m} f V}{4r} \sqrt{1+u^2} \right) \\ & + u \left(\lambda_1 \left(\frac{\dot{m} f V}{4r} \frac{u}{\sqrt{1+u^2}} - 2\pi r P \right) - \frac{\dot{m} f V^2}{4rT} \frac{u}{\sqrt{1+u^2}} \right) \end{aligned}$$

or

$$\mathcal{H} = \frac{\dot{m} f V^2}{4rT} \sqrt{1+u^2} - \lambda_1 \frac{\pi r f \rho V^2}{4} \sqrt{1+u^2} + \frac{u^2}{\sqrt{1+u^2}} \left(\lambda_1 \frac{\dot{m} f V}{4r} - \frac{\dot{m} f V^2}{4rT} \right).$$

Putting all of the terms on a common denominator $\sqrt{1+u^2}$ leads to

$$\mathcal{H} = \frac{1}{\sqrt{1+u^2}} \left(\frac{\dot{m} f V^2}{4rT} \left(1+u^2\right) - \lambda_1 \frac{\dot{m} f V}{4r} \left(1+u^2\right) + u^2 \left(\lambda_1 \frac{\dot{m} f V}{4r} - \frac{\dot{m} f V^2}{4rT} \right) \right),$$

which can be simplified to yield

$$\mathcal{H} = \frac{1}{\sqrt{1+u^2}} \left(\frac{\dot{m} f V^2}{4rT} - \lambda_1 \frac{\dot{m} f V}{4r} \right) = \frac{\dot{m} f V}{4r\sqrt{1+u^2}} \left(\frac{V}{T} - \lambda_1 \right). \tag{2.53}$$

The Hamiltonian in this problem formulation is not an explicit function of z. Therefore, $\mathcal{H} =$ constant is an integral of the system for an optimal state [36, 37]. Using this and Equation (2.53) we have

$$\mathcal{H} = \frac{\dot{m} f V}{4r\sqrt{1+u^2}} \left(\frac{V}{T} - \lambda_1 \right) = \text{constant}. \tag{2.54}$$

To solve the differential equations governing the spatial evolution of λ_1 and λ_2, we need to find $\partial\mathcal{H}/\partial\dot{M}$ and $\partial\mathcal{H}/\partial r$. Differentiation of the Hamiltonian with respect to $\dot{M}$ requires use of the chain rule, since $\mathcal{H}$ has been formulated in terms of ρ, V, P and T, all of which $\dot{M}$ depends on either explicitly or implicitly. To reduce the number of differentiations needed, $T = P/\rho R$ is substituted out of the Hamiltonian with the use of the ideal gas equation of state. Applying the chain rule when differentiating $\mathcal{H}$ with respect to $\dot{M}$ then gives

$$\frac{\partial\mathcal{H}}{\partial\dot{M}} = \frac{\partial\mathcal{H}}{\partial\rho}\frac{\partial\rho}{\partial\dot{M}} + \frac{\partial\mathcal{H}}{\partial V}\frac{\partial V}{\partial\dot{M}} + \frac{\partial\mathcal{H}}{\partial P}\frac{\partial P}{\partial\dot{M}}. \tag{2.55}$$

With $\dot{M} = A\left(P + \rho V^2\right)$, assuming that the Implicit Function Theorem holds [39], we have

$$\frac{\partial\dot{M}}{\partial\rho} = AV^2 \implies \frac{\partial\rho}{\partial\dot{M}} = \frac{1}{AV^2}, \tag{2.56}$$

$$\frac{\partial\dot{M}}{\partial V} = 2\rho AV = 2\dot{m} \implies \frac{\partial V}{\partial\dot{M}} = \frac{1}{2\dot{m}}, \tag{2.57}$$

$$\frac{\partial\dot{M}}{\partial P} = A \implies \frac{\partial P}{\partial\dot{M}} = \frac{1}{A}. \tag{2.58}$$

It remains to find the partial derivatives of $\mathcal{H}$ with respect to ρ, V and P. Performing the differentiation, one arrives at the following expressions:

$$\frac{\partial\mathcal{H}}{\partial\rho} = \frac{\dot{m}fRV^2}{4rP}\sqrt{1+u^2} - \frac{\lambda_1\pi rfV^2}{4}\sqrt{1+u^2}, \tag{2.59}$$

$$\frac{\partial\mathcal{H}}{\partial V} = \frac{\dot{m}fR\rho V}{2rP}\sqrt{1+u^2} - \frac{\lambda_1\pi rf\rho V}{2}\sqrt{1+u^2}, \tag{2.60}$$

$$\frac{\partial\mathcal{H}}{\partial P} = 2\pi r\lambda_1 u - \frac{\dot{m}fR\rho V^2}{4rP^2}\sqrt{1+u^2}. \tag{2.61}$$

Finally, after inserting the expressions in Equations (2.56)–(2.61) into Equation (2.55) and doing a little bit of algebra, we arrive at

$$\frac{\partial\mathcal{H}}{\partial\dot{M}} = -\frac{d\lambda_1}{dz} = \sqrt{1+u^2}\left[\frac{\dot{m}fR}{4\pi r^3P^2}\left(2P - \rho V^2\right) - \frac{\lambda_1 f}{2r}\right] + \frac{2\lambda_1 u}{r}. \tag{2.62}$$

To establish the governing equation for λ_2, we must determine $\partial\mathcal{H}/\partial r$. If the Hamiltonian was formulated explicitly in terms of $\dot{M}$ and r, we could partial differentiate $\mathcal{H}$ with respect to r while keeping the other variables in the expression constant. Because $\mathcal{H}$ is a function of ρ, V, P and T though, there are some implicit relations that need to be considered. With the algebraic relations Equations (2.11)–(2.14) derived at the end of Section 2.1, one can solve explicitly for all of the variables ρ, V, P and T in terms of $\dot{M}$ and r. The resulting expressions show that only ρ and P are implicit functions of r when formulated this way, while V and T only depend on $\dot{M}$. This means that upon differentiation of $\mathcal{H}$ with respect to r, we cannot keep P constant. With the relations

$$\rho = \frac{\dot{m}}{\pi r^2 V},$$
$$P = \frac{\dot{M}}{\pi r^2} - \rho V^2 = \frac{1}{\pi r^2}\left(\dot{M} - \dot{m}V\right),$$

together with the knowledge that V is not implicitly a function of r, it follows that

$$\frac{\partial\rho}{\partial r} = -\frac{2\dot{m}}{\pi r^3 V} = -\frac{2\rho}{r},$$
$$\frac{\partial P}{\partial r} = -\frac{2}{\pi r^3}\left(\dot{M} - \dot{m}V\right) = -\frac{2P}{r}.$$

To check that these are correct expressions, we can verify that $\partial\dot{M}/\partial r$ is indeed equal to zero, which it should be since $\dot{M}$ and r are supposed to be independent variables in the current problem formulation:

$$\begin{aligned}\frac{\partial \dot{M}}{\partial r} &= \frac{\partial}{\partial r}\left(\pi r^2\left(P+\rho V^2\right)\right)\\ &= 2\pi r\left(P+\rho V^2\right)+\pi r^2\left(\frac{\partial P}{\partial r}+\frac{\partial \rho}{\partial r}V^2\right)\\ &= 2\pi r\left(P+\rho V^2\right)+\pi r^2\left(-\frac{2P}{r}-\frac{2\rho}{r}V^2\right)\\ &= 2\pi r\left(P+\rho V^2\right)-2\pi rP-2\pi\rho V^2=0.\end{aligned}$$

Finally, we can now establish the governing equation for λ_2 by partial differentiation of the Hamiltonian with respect to r

$$\begin{aligned}\frac{\partial \mathcal{H}}{\partial r}=-\frac{d\lambda_2}{dz} &= -\frac{\dot{m}fV^2}{4r^2T}\sqrt{1+u^2}+\lambda_1\left(2\pi Pu+2\pi ru\frac{\partial P}{\partial r}+\frac{\dot{m}fV}{4r^2}\sqrt{1+u^2}\right)\\ &= \frac{\dot{m}fV\sqrt{1+u^2}}{r^2}\left(\lambda_1-\frac{V}{T}\right)+2\pi\lambda_1 Pu+2\pi r\lambda_1 u\frac{-2P}{r}\\ &= \frac{\dot{m}fV\sqrt{1+u^2}}{r^2}\left(\lambda_1-\frac{V}{T}\right)-2\pi\lambda_1 Pu.\end{aligned}$$

Solving for the Optimal Control Variable

The stationarity condition of Equation (2.51) is an algebraic equation to be solved for u when the variables ρ, V, P and the Lagrange multiplier functions λ_1 and λ_2 are known quantities. Defining the quantities

$$a=\frac{\dot{m}fV^2}{4rT},\ b=2\pi rP,\ c=\frac{\dot{m}fV}{4r},$$

and using these in Equation (2.51), while at the same time multiplying the equation with $\sqrt{1+u^2}$, results in

$$au+\lambda_1\left(b\sqrt{1+u^2}-cu\right)+\lambda_2\sqrt{1+u^2}=0,$$

which can be rearranged to

$$\left(\lambda_1 b+\lambda_2\right)\sqrt{1+u^2}=\left(\lambda_1 c-a\right)u.$$

Letting $k_1=\lambda_1 b+\lambda_2$ and $k_2=\lambda_1 c-a$, we have

$$k_1\sqrt{1+u^2}=k_2 u. \tag{2.63}$$

At first sight, it could seem straightforward to square both sides and solve for u^2 to obtain an equation for the control variable. Doing so, however, reveals a subtlety to the existence of solutions to Equation (2.63):

$$\begin{aligned}k_1^2\left(1+u^2\right)&=k_2^2u^2\\ u^2\left(k_2^2-k_1^2\right)&=k_1^2\end{aligned}$$

and given $k_2^2-k_1^2\neq 0$ we can write

$$u^2=\frac{k_1^2}{k_2^2-k_1^2}=\frac{1}{k_3^2-1},\ \text{with } k_3=k_2/k_1,$$

which leads to

$$u = \pm \frac{1}{\sqrt{k_3^2 - 1}}.$$

Evidently, if $|k_3| \leq 1$, no solutions for u exist. One would also need to find a way to determine which sign of u should be chosen when taking the square root, making this approach problematic.

A work-around is to use Equation (2.54). We have from the stationarity condition (Equation (2.51)) that

$$\frac{u}{\sqrt{1+u^2}} \left(\frac{\dot{m} f V^2}{4rT} - \lambda_1 \frac{\dot{m} f V}{4r} \right) + 2\pi r P \lambda_1 + \lambda_2 = 0$$

or

$$\frac{\dot{m} f V}{4r\sqrt{1+u^2}} \left(\frac{V}{T} - \lambda_1 \right) u + 2\pi r P \lambda_1 + \lambda_2 = 0.$$

Observe that the factor multiplied with u is the $\mathcal{H}$ = constant expression from Equation (2.54). The above equation is thus readily solved to yield the optimal control variable

$$u = -\frac{2\pi r P \lambda_1 + \lambda_2}{\mathcal{H}}, \tag{2.64}$$

given that $\mathcal{H} \neq 0$.

Chapter 3

Methodology

The programmed implementation of the pipe flow model that has been developed is outlined at the start of this chapter, together with a reference case established for comparison with the optimization results. All of the code implemented is original and developed by the author, apart from a few built-in MATLAB functions which are cited in the text. The second section of this chapter begins with covering the different sets of boundary conditions used in the optimization, where two different optimization cases are defined. Then follows details on the numerical constrained optimization performed, after which the implementation of the optimal control theory problem formulation is covered. At the end of the chapter is a section dedicated to methods used for model validation and numerical error analyses of the results.

3.1 Pipe Flow Model Implementation and Reference Case

With the geometry and flow state set at the inlet of the pipe together with a profile for the slope of the radius, the governing equations of the pipe flow model constitute an initial value problem that can be solved by integration. This was used to establish a reference case for the optimization performed. Figure 3.1 shows an illustration of the geometry used to establish the reference case, which is a typical air ejector diffuser section chosen based on the motivation behind this thesis work. The details of the reference case can be found in Table 3.1. Subscript 0 denotes values at the inlet of the pipe ($z_0 = 0$) and subscript f denotes values at the outlet of the pipe ($z_f = L$). The values of L, r_0 and r_f were chosen based on the geometry of the diffuser section of the air ejector studied by Dandani *et al.* [40]. The u profile of this diffuser geometry was a constant $u = 0.13$.

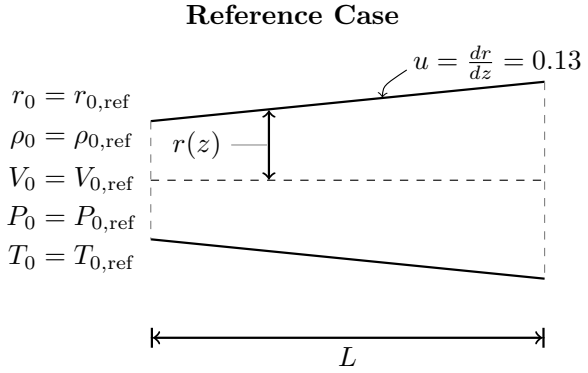

Figure 3.1: An illustration of the geometry used to establish a reference case for the optimization. Inspired by the geometry of the air ejector studied in [40].

Variable	Symbol	Value
Inlet Density	ρ_0	0.594 kg/m^3
Inlet Velocity	U_0	100 m/s
Inlet Pressure	P_0	$0.5 \cdot 10^5$ N/m^2
Inlet Temperature	T_0	293.15 K
Inlet Radius	r_0	0.024 m
Outlet Radius	r_f	0.0578 m
Mass Flow Rate	$\dot{m}$	0.0108 kg/s
Slope of the Radius	u	0.13

Table 3.1: Values of the inlet variables, outlet radius, the total mass flow rate and the constant value of the slope of the radius profile used in the reference case. The values were chosen to represent air flow in a typical ejector in a regime where the assumption of an ideal gas holds well.

The initial value problem of the governing equations with the reference case inlet conditions and u profile were solved with numerical integration. This was done with the classical fourth-order Runge-Kutta integration scheme, using the function *ode*45 in MATLAB [41]. The function performs adaptive step-size integration, using a fifth-order method to control the step size. The same function was used to calculate the total entropy production by integration, implementing the expression inside the integral as the right-hand side of a differential equation and setting zero as the initial condition. Numerical tolerances for the numerical integrator was to 1×10^{-10}, because such high accuracies did not lead to high computational costs for the numerical integration solver used.

Property	Symbol	Value
Pipe Length	L	0.26 m
Fanning Friction Factor	f	0.1
Heat Capacity	c_p	1005 J/kgK
Specific Gas Constant	R	287 J/kgK
Reference Temperature	T_{ref}	298 K

Table 3.2: System constants and fluid properties of air.

Table 3.2 summarizes all system constants and fluid properties used in the model implementation.The value of the Fanning friction factor was set as a constant equal to 0.1, which represents a fairly rough pipe. For the reference case radius profile values, the friction factor value is representative of a pipe with wall roughness similar to concrete [42]. This was chosen to enhance the effects of friction in the pipe to facilitate analysis and the resulting discussion. A constant friction factor value implies an assumption of fully developed turbulent flow, as the friction factor is by no means constant for all flow regimes. To support the assumption of turbulent flow, the Reynolds number throughout the pipe in the reference case was in the order of 1×10^5, which is considered completely turbulent for the wall roughness used here.

For calculations of specific enthalpy, a reference temperature is needed and a reference enthalpy must be set at that temperature. For an ideal gas, the choice of references can be arbitrary. The reference temperature was here set to $T_{\text{ref}} = 298$ K, representing ambient conditions. At this temperature, the reference enthalpy was set equal to zero for the sake of simplicity, since this choice can be arbitrary.

The specific heat capacity of the air was assumed to be constant. It is in reality a function of temperature [5], but the assumption of c_p being constant leads to negligible errors here due to low variations in temperature.

3.2 Optimization

This section begins with the two boundary condition cases used in the optimization performed. Then follows details of the implementation of the numerical constrained optimization, after which the method implemented to solve the boundary value problem of the optimal control theory formulation is covered.

3.2.1 Optimization Cases and Boundary Conditions

The optimization done in this work considered two optimization cases. See Figure 3.2 for an illustration of the two cases. Both cases had equal inlet boundary conditions. The difference between the optimization cases was the boundary condition at the outlet. One case considered a given pipe outlet radius, with the outlet state of the fluid being free to vary. In the second case the pressure at the outlet was set as a boundary condition, with the rest of the outlet variables being free to vary. For both of the cases, the outlet boundary condition was set to the reference case outlet condition. This means that $r(z = L) = r_f = r_{f,\text{ref}}$ was set for the radius boundary condition case, and $P(z = L) = P_f = P_{f,\text{ref}}$ was set for the pressure boundary condition case. The case of using the outlet

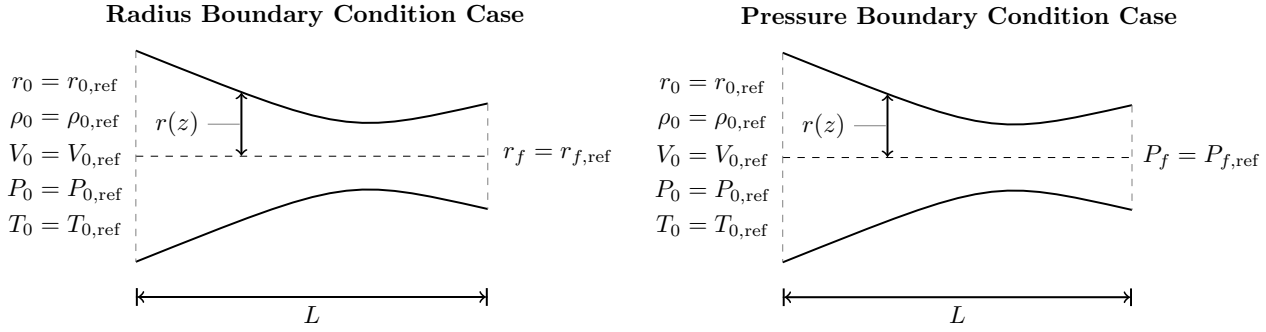

Figure 3.2: Illustrations of the two sets of boundary conditions considered for optimization. The left figure illustrates the radius boundary condition case, where the final radius r_f of the pipe is set. The right figure illustrates the pressure boundary condition case, where the outlet pressure P_f is set. For both of the cases, all of the inlet conditions were equal to the reference case values. The length of the pipe is L and $r(z)$ is the radius as a function of the axial coordinate z.

radius as a boundary condition was motivated by a type of design problem, where the outlet radius needs to match a certain criteria. This could for example be because a new pipe section follows after the diffuser if it is used in an application. The pressure boundary condition case was motivated by the curiosity regarding whether minimization of entropy production given an outlet pressure would yield a radius profile that leads to a higher velocity at the outlet of the ejector. This is expected by the theory developed in Chapter 2. Setting both the radius and the pressure at the outlet would lead to an over-specified problem for the model developed here, which is why this boundary condition choice was of no interest.

For both of the optimization cases, all of the inlet variables were set according to the values at the inlet in the reference case:

$$\begin{aligned} \rho_0 &= \rho_{0,\text{ref}}, \\ U_0 &= U_{0,\text{ref}}, \\ P_0 &= P_{0,\text{ref}}, \\ T_0 &= T_{0,\text{ref}}, \\ r_0 &= r_{0,\text{ref}}. \end{aligned} \tag{3.1}$$

The boundary conditions for the optimal control theory formulation depend on which boundary conditions that are given for the state variables $\dot{M}$ and r. For both of the optimization cases all inlet variables were set, such that $\dot{M}_0$ and r_0 are given. Because of this, both λ_1 and λ_2 are unspecified at the inlet [37]. For the boundary condition case where the outlet radius r_f is specified, $\lambda_{2,f}$ is unspecified. Letting the momentum flow rate at the outlet vary freely, we must require that $\lambda_{1,f} = 0$ owing to the transversality condition.

For the pressure boundary condition case, both $\dot{M}_f$ and r_f are unspecified. Because the pressure $P_f = P_{f,\text{ref}}$ is set at the outlet, an extra equation is added to the optimal control theory formulation [37]:

$$\nu\psi = \nu\left(P_f - P_{f,\text{ref}}\right) = 0,$$

with the extra constant ν available in order to satisfy the pressure boundary condition. The boundary conditions for λ_1 and λ_2 at the outlet then follow from the transversality conditions

$$\begin{aligned} \lambda_{1,f} &= \nu \left.\frac{\partial\psi}{\partial\dot{M}_f}\right|_{z=L} = \nu \left.\frac{\partial\psi}{\partial P_f}\frac{\partial P_f}{\partial\dot{M}_f}\right|_{z=L} = \frac{\nu}{\pi r_f^2}, \\ \lambda_{2,f} &= \nu \left.\frac{\partial\psi}{\partial r_f}\right|_{z=L} = \nu \left.\frac{\partial\psi}{\partial P_f}\frac{\partial P_f}{\partial r_f}\right|_{z=L} = -\frac{2\nu P_f}{r_f}. \end{aligned}$$

3.2.2 Numerical Constrained Optimization

The constrained minimization problem formulated in Section 2.3.1 was discretized and solved iteratively using the MATLAB function *fmincon* [43]. An interior-point algorithm with barrier functions to handle the constraints was used. The solver requires an initial guess, for which the variable profiles from solving the reference case presented in the previous section were chosen. Numerical bounds for the variables were set to avoid completely unphysical results. See Table 3.3 for the values of the bounds. These bounds are simply the maximum value that the variables are allowed to attain at any point of the discretization grid. The reason behind the particular choice of the bounds for u were that these values pertain to a slope of approximately 20°. A larger diffuser angle than this is considered unlikely to be applicable in practice, as this could lead to several detrimental flow features [44, 45].

When solving the problem numerically, the axial coordinate z of the pipe was discretized as a grid of $k = 1, \ldots, N$ points. The variables and their derivatives had to be discretized. Derivatives were discretized with the classical upwind scheme, such that for a variable ϕ, the derivative at grid point k was discretized as

$$\left.\frac{d\phi}{dz}\right|_k \approx \frac{\phi_k - \phi_{k-1}}{z_k - z_{k-1}}$$

between two grid points z_k and z_{k-1}. The upwind scheme is only a first-order accurate scheme, but it is very stable [46]. For variables appearing in the equations, the mean of the variable value between the two grid points was used

$$\phi \approx \phi_{m,k} = (\phi_k + \phi_{k-1})/2.$$

Variable [Unit]		Lower Bound	Upper Bound
ρ	[kg/m^3]	0.001	100
V	[m/s]	1.0×10^{-7}	1000
P	[N/m^2]	1000	1.0×10^{7}
T	[K]	253.15	773.15
r	[m]	1.0×10^{-6}	1
u	[-]	-0.36	0.36

Table 3.3: Numerical lower and upper bounds for the values of the variables when performing numerical constrained optimization.

The continuity equation on differential form is used as an example to illustrate the method. The exact equation reads

$$\frac{1}{\rho}\frac{d\rho}{dz} + \frac{1}{A}\frac{dA}{dz} + \frac{1}{V}\frac{dV}{dz} = 0$$

and the discretized version is

$$\frac{1}{\rho_{m,k}}\frac{\rho_k - \rho_{k-1}}{z_k - z_{k-1}} + \frac{1}{A_{m,k}}\frac{A_k - A_{k-1}}{z_k - z_{k-1}} + \frac{1}{V_{m,k}}\frac{V_k - V_{k-1}}{z_k - z_{k-1}} = 0 \quad \text{for} \quad k = 2, \ldots, N,$$

for a grid discretized with a number of N points. Subscript m, k denotes the mean of the two values of a variable at the points z_k and z_{k-1}. The choice of discretization method was inspired by Johannessen [3] who reported successful application of the same technique to several problems where process equipment was optimized with non-equilibrium thermodynamics theory, using a similar numerical optimization method.

The discretized versions of the governing equations together with the boundary conditions were used as equality constraints in the optimization routine. Since the objective function is a function of six variables, the total number of variables were $6N$. With five constraints to be satisfied at $N - 1$ grid points in addition to six boundary condition constraints, the total number of constraints was $5(N - 1) + 6$.

The objective function (the total entropy production) was discretized over the grid points $k = 1, \ldots, N$ and the total entropy production was determined by numerical integration of these function values with the trapezoidal rule, using the MATLAB function *trapz* [47].

A total number of $N = 150$ grid points were used, leading to a grid solution of $\Delta z = z_k - z_{k-1} = 0.0017$. The choice of grid points was a compromise between accuracy and computational cost. At this number the calculation of the total entropy production had reached a constant value, indicating that the accuracy of the grid was satisfactory. It was therefore chosen not to increase the grid size further to save computational time.

The numerical tolerance of the solver used was set to 1×10^{-5}. The solver calculates a first-order optimality measure based on the gradient of the objective function with respect to the variables and iterates towards a point of lower first-order optimality measure, given that the point lies in a feasible direction. A feasible direction is any direction in the solution space in which changes in the variables do not violate the problem constraints. If the first-order optimality measure is lower than the tolerance set, the solver concludes that a local minimum is found. The tolerance set was deemed accurate enough to indicate that a local minimum has been found, without demanding too much computational time. In the case that the solver stops for another reason than finding a local

minimum (e.g. that step-sizes are smaller than the step-size tolerance set), an exit message is provided by the solver. For all of the numerical optimization results discussed in Chapter 1, the exit message was that a local minimum was found.

Poor scaling of an optimization problem may lead to problems with finding a solution numerically through iteration [35]. With the order of magnitude of the variables differing greatly, problems during optimization could occur since the components of the step-size to be taken in a feasible direction would influence the step in very different ways. Because poor scaling can be problematic, all of the variables were non-dimensionalized. The scale for each variable was chosen to be the value of the respective variable at the inlet of the pipe. The objective function (the total entropy production) was non-dimensionalized with the total entropy production calculated for the reference case.

3.2.3 Optimal Control Theory

The equation set derived in Section 2.3.2 consists of four differential equations and one algebraic equation. The four differential equations constitute a two-point boundary value problem. The two-point boundary value problem (BVP) was solved using a collocation method, with the MATLAB function *bvp5c* [48]. It approximates the solution curves with cubic polynomials and chooses adaptively the number of grid points to be used. The tolerance of the solver was set to 1×10^{-3} to reduce computational time. The collocation method requires a reasonably good initial guess. In this work, the profiles resulting from the numerical optimization outlined in Section 3.2.2 were used as an initial guess for the flow variable profiles. This choice was inspired by previous work where similar optimization routines were employed [3, 9, 11].

An initial guess for the profiles of the multiplier functions λ_i was generated using numerical constrained minimization. The objective function used in the minimization was the sum of squared errors (SSE) of the Hamiltonian

$$\mathcal{H}_{\mathrm{SSE}} = \sum_{k=1}^{N} \left(\mathcal{H}_k - \overline{\mathcal{H}} \right)^2, \tag{3.2}$$

where $\overline{\mathcal{H}}$ is the mean of the values $\mathcal{H}_k$ of the Hamiltonian at the grid points $k = 1, \ldots, N$:

$$\overline{\mathcal{H}} = \frac{1}{N} \sum_{k=1}^{N} \mathcal{H}_k,$$

with N being the total number of grid points. To calculate the Hamiltonian at every grid point the flow variables are needed. The results from the numerical optimization of the radius profile were used for this. The constraints of the minimization problem were the governing equations of λ_i. The optimization problem to find the initial guess of λ_i was then

$$\begin{gathered} \min_{\lambda_i} \mathcal{H}_{\mathrm{SSE}} \\ \text{subject to} \\ \frac{d\lambda_1}{dz} + \frac{\partial \mathcal{H}}{\partial \dot{M}} = 0, \\ \frac{d\lambda_2}{dz} + \frac{\partial \mathcal{H}}{\partial r} = 0, \end{gathered}$$

with the partial derivatives of $\mathcal{H}$ derived in Section 2.3.3. This method of finding an initial guess for λ_i was motivated by the fact that the Hamiltonian of the problem is autonomous, and should therefore be constant along an optimal trajectory [37]. For a constant value of $\mathcal{H}$ Equation (3.2) would be equal to zero.

The details of the BVP solution procedure implemented were as follows. With the initial profile guesses for the flow variables and the multiplier functions, the solver was initiated. The BVP solver then solved the algebraic equation

$$u = -\frac{2\pi r P \lambda_1 + \lambda_2}{\mathcal{H}} \tag{3.3}$$

and the governing differential equations of $\dot{M}$, r, λ_1 and λ_2 simultaneously over the entire discretization grid. Additionally, the solver calls a boundary condition function which was implemented, so that the variables of the solution are ensured to satisfy the boundary conditions of the problem. The solution procedure continues iteratively until either a solution is found or a problem with solution of the equations occurs.

To be able to calculate u with Equation (3.3), the value of the constant Hamiltonian is needed. The function *bvp5c* used to solve the BVP has functionality which supports solving a BVP with an unknown constant parameter, given that an extra boundary condition is provided. Using the solver with $\mathcal{H}$ as an unknown constant parameter, the extra boundary condition added to the problem was determined by using the Hamiltonian expression derived in Section 2.3.3:

$$\mathcal{H} = \frac{\dot{m} f V}{4r\sqrt{1+u^2}} \left(\frac{V}{T} - \lambda_1 \right) = \text{constant}.$$

Evaluating this expression at $z = L$ yields

$$\mathcal{H}_{f,1} = \frac{\dot{m} f V}{4r\sqrt{1+u^2}} \left(\frac{V}{T} - \lambda_1 \right) \Bigg|_{z=L},$$

which should match the calculation of the Hamiltonian at $z = L$ with the original expression for $\mathcal{H}$, denoted $\mathcal{H}_{f,2}$:

$$\mathcal{H}_{f,2} = \left(\sigma + \lambda_1 \frac{d\dot{M}}{dz} + \lambda_2 \frac{dr}{dz} \right) \Bigg|_{z=L}.$$

The extra boundary condition provided to the solver was thus

$$\mathcal{H}_{f,1} = \mathcal{H}_{f,2}.$$

3.3 Error Analysis and Implementation Consistency

In this section, techniques used for error analysis and check of model implementation consistency are explained. Whenever it is referred to the standard deviation of a variable ϕ, this was calculated as [49]

$$\sqrt{\frac{1}{N-1} \sum_{k=1}^{N} (\phi_k - \mu)},$$

where ϕ_k is element k of an array totaling N elements, and μ is the mean

$$\mu = \frac{1}{N} \sum_{k=1}^{N} \phi_k.$$

This is the mean value referred to in the tables presented in Chapter 4. When a table refers to the maximum value of a quantity ϕ, this is simply the highest value of all ϕ_k.

3.3.1 Conserved Properties and Thermodynamics

Conservation of mass and energy as well as consistency in entropy calculations were checked for all numerical solutions. For a numerical solution where the variables were arrays of N elements, the mass flow rate and stagnation enthalpy

$$\dot{m}_k = \rho_k A_k V_k,$$
$$h_{s,k} = c_p \left(T_k - T_{\text{ref}}\right) + V_k^2/2,$$

were calculated at every grid point $k = 1, \ldots, N$. The deviations from the mean value were then calculated as

$$D_m = \dot{m}_k - \overline{\dot{m}},$$
$$D_h = h_{s,k} - \overline{h},$$

and the maximum of this deviation was checked. Since both $\dot{m}$ and h_s should be constant, this max deviation should be in the order of the tolerance of the numerical calculations. This would then ensure that mass and energy were properly conserved for the solutions obtained.

As mentioned earlier, a way to check the consistency of the expression for the local entropy production derived in Section 2.2.2 is to calculate the total entropy change with an entropy balance over the entirety of the pipe

$$\dot{m}(s_f - s_0) = \dot{m}\Delta s, \tag{3.4}$$

and compare this with the total entropy production calculated by integration of the local entropy production. These two calculations should give the same result if the entropy production is derived and implemented correctly [2]. In Equation (3.4), subscript f denotes the pipe outlet and 0 denotes the pipe inlet. The entropy difference Δs is calculated with the thermodynamic relation derived in Section 2.2.3, repeated here for clarity:

$$\Delta s = s_f - s_0 = c_p \ln \frac{T_f}{T_0} - R \ln \frac{P_f}{P_0}.$$

This entropy difference was compared to the total entropy production

$$\sigma_{\text{tot}} = \int_0^L \sigma dz$$

and the metric used to quantify the error was the relative deviation in percentage between the two

$$D_s = \frac{\Delta s - \sigma_{\text{tot}}}{\Delta s} \times 100\%.$$

For the optimization results, the above thermodynamic consistency check was not only applied to the solution obtained directly from numerical optimization . Additionally, the u profile of the optimization solution was used as an input to solve the initial value problem that the ODEs of the pipe flow and the inlet conditions constitute. This is similar to what was done to establish the reference case, the only difference being that the input u profile is now the one resulting from optimization. This re-integration was performed for two reasons. First, to check that the flow variable and radius profiles of the optimization solution are reproduced by the ODE solver for the optimal u profile, serving as a model consistency check. If completely different flow variable and radius profiles resulted from the re-integration, it would indicate problems with the model or the implementation. Second, to reduce numerical errors. The errors are reduced because the numerical optimization is performed over an equidistant grid with a low-order-of-accuracy discretization scheme, whereas the ODE integrator used employs an adaptive step-size algorithm. It places more grid points in the vicinity of high gradients, leading to more accurate results. Since the ODE solver uses adaptive step-sizing, the optimal u profile used to re-integrate the equations had to be interpolated, which was done with cubic spline interpolation using the MATLAB function *spline* [50].

3.3.2 Partial Differentiation

The correctness of the analytical expressions of the partial derivatives of the Hamiltonian that were derived in Section 2.3.3 was checked numerically. To illustrate the method used, $\partial\mathcal{H}/\partial u$ will be used as an example. A relative perturbation of u, denoted δ_u, was done while holding the other variables and the multiplier functions constant. The Hamiltonian was then calculated at $u + \delta_u$ and $u - \delta_u$, denoted $\mathcal{H}_+$ and $\mathcal{H}_-$, respectively. A central difference approximation of the partial derivative was then calculated as

$$\frac{\partial\mathcal{H}}{\partial u} \approx \frac{\mathcal{H}_+ - \mathcal{H}_-}{2\delta_u}$$

and compared with the numerical value of the implementation of the analytical expression. This should lead to an error in the order of the tolerance of the numerical calculations if the analytical derivative expressions are correct.

When performing the perturbations, it is important to correctly account for the variable dependencies to ensure that only valid perturbations are made. Valid here means that the perturbed set of variables satisfy the governing equations, and that either $\dot{M}$ or r are kept constant whenever the other is perturbed. When perturbing $\dot{M}$, r was automatically kept constant. When perturbing r, the partial derivative expressions derived in Section 2.3.3 were used to perturb ρ and P so that $\dot{M}$ was kept constant. For a relative perturbation δ_r of the radius r, the perturbations of ρ and P were calculated as

$$\delta_\rho = \frac{\partial\rho}{\partial r}\delta_r,$$
$$\delta_P = \frac{\partial P}{\partial r}\delta_r.$$

When calculating the numerical derivatives, the relative perturbation of the respective variable was equal to 1×10^{-5}. For example, if a perturbation of u was made at a point where $u = u_p$, the perturbation was of size $\delta_u = u_p \times 10^{-5}$.

Chapter 4

Results and Discussion

This chapter starts with a presentation of the radius profile, flow variable profiles and the local entropy production calculated for the reference case. Next, results from numerical constrained optimization are presented. Local minima were found with the optimization Numerical constrained optimization for the radius boundary condition case will be covered first, followed by the pressure boundary condition case. For the numerical constrained optimization results, results from the first case are referred to as Numerical Optimization Radius (NOR), and results pertaining solutions of the second case are referred to as Numerical Optimization Pressure (NOP). Results from the optimal control theory optimization are discussed at the end of the chapter. The nature of the solutions and practical consequences of the results are discussed, comparing the optimization results with the reference case. For the optimal control theory part, solution of the problem formulated was unsuccessful. Results, error analyses and probable sources of error are discussed.

For all results, only the radius profile for the upper half of the pipe is considered. The profile of the lower half follows from radial symmetry.

4.1 Reference Case

With the inlet conditions and the slope of the radius specified in Section 3.1, the variable profiles throughout the pipe were found by integration. The radius profile and its slope for the reference case are illustrated in Figure 4.1.

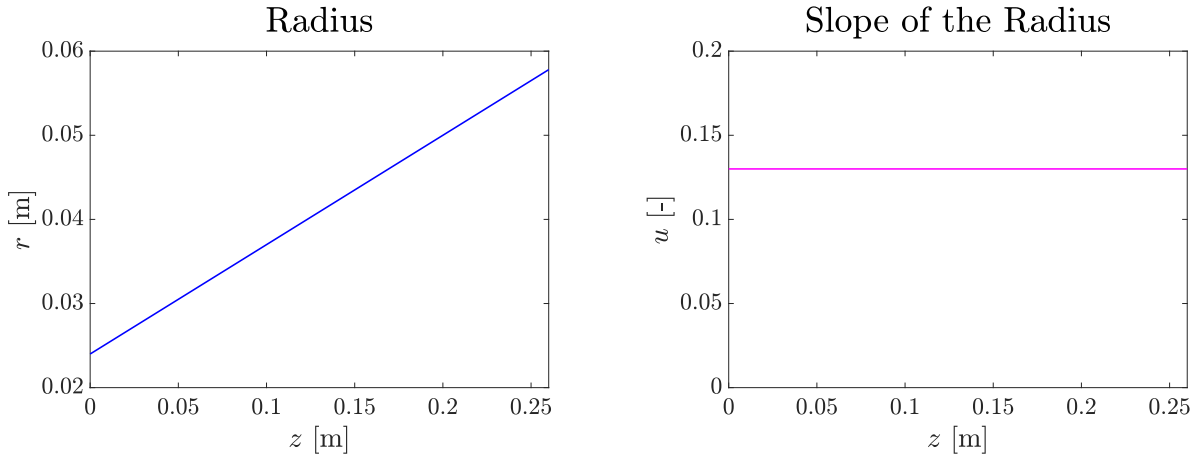

Figure 4.1: Radius and slope of the radius profile for the reference case.

Flow variable profiles are shown in Figure 4.2. A pressure increase is observed as the fluid is expanded in the diffuser geometry. The velocity decreases towards the outlet as the area increases, and the velocity decrease is also affected by the momentum loss cause by the friction forces. Changes in density and temperature are small, in the absence of strong compressibility effects and heat transfer [51]. It is observed that the velocity change is orders of magnitudes larger than the changes in the other variables. This is because the orders of magnitude of the velocity and density result in a dynamic pressure which is one to two orders of magnitude smaller than the pressure, such that small changes in the pressure leads to large changes in the velocity through the momentum equation.

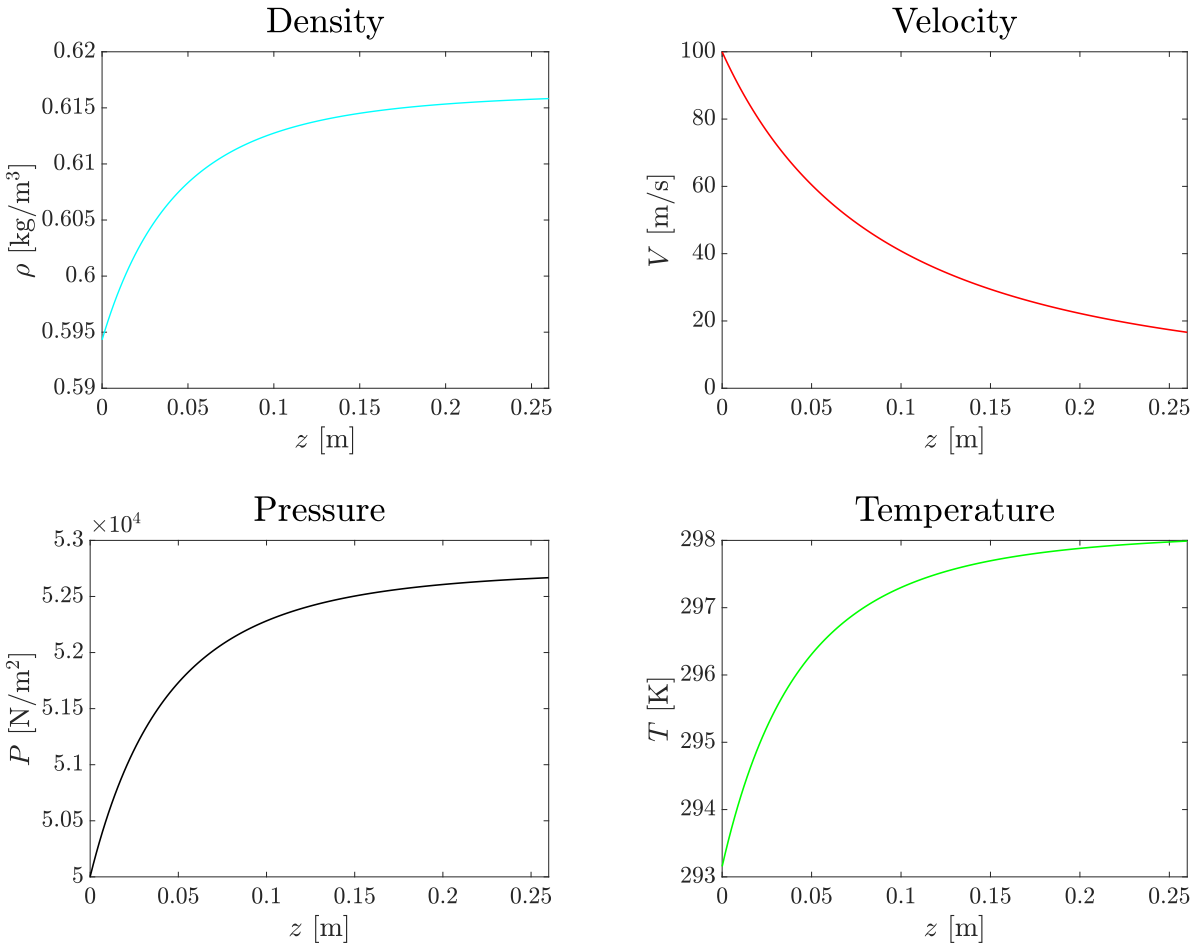

Figure 4.2: Flow variable profiles for the reference case.

The total entropy production for the reference case equalled 0.165 W/K. The local entropy production of the flow in the reference case is plotted in Figure 4.3. It is observed that the entropy production is by no means equipartitioned, or in other words is not constant. Since previous research as mentioned in Chapter 1 has characterized constant entropy production as either the state of minimum entropy production or a good approximation to it [3, 6–9], it can be inferred from the profile in Figure 4.3 that there exists a radius profile design which leads to less total entropy production than for the reference case.

In Table 4.1, numerical values for the consistency checks performed for the reference case are presented. We observe that mass and energy is conserved, with the max error of the energy balance being within machine precision. The relative deviation between the macroscopic entropy balance and total entropy production is of low order, but we should see very low errors for this metric because

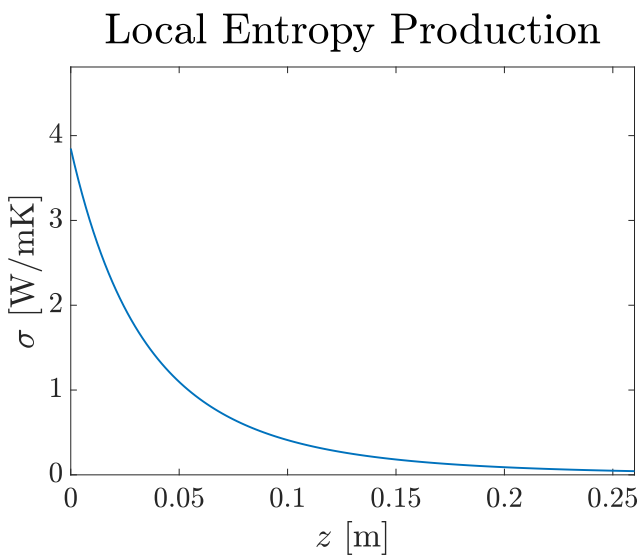

Figure 4.3: Local entropy production for the reference case.

the total entropy production and the macroscopic entropy balance are supposed to be identical. A check of convergence was performed by increasing the tolerance of the ODE solver with one order of magnitude. This lead to one order of magnitude higher accuracy in the entropy calculations, indicating that the derivation and implementation of the entropy production term for the model is consistent.

Reference Case

Consistency Check	Quantity	Value
Mass Conservation	$\max\{D_m\} = \max\{\dot{m}_i - \overline{\dot{m}}\}$	0
Energy Conservation	$\max\{D_h\} = \max\{h_{s,i} - \overline{h_s}\}$	8.9×10^{-11} J/kg
Entropy Balance	Δs	0.1648 W/K
Total Entropy Production	σ_{tot}	0.1648 W/K
Relative Deviation	$D_s = \dfrac{\Delta s - \sigma_{\text{tot}}}{\Delta s} \times 100\%$	-2.0×10^{-5} %

Table 4.1: Numerical values for the consistency checks performed for the reference case. The deviations used in the tables are described in Section 3.3.1

4.2 Numerical Constrained Optimization

The results of the numerical constrained optimization (hereafter referred to as numerical optimization) using the total entropy production as an objective function are presented in this section. First, the results of the error analysis and consistency check are covered to ensure that the results discussed are consistent with the model implementation. Then, results from the Numerical Optimization Radius (NOR) case are discussed. This is the case where the outlet radius of the pipe was set as a boundary condition. Next follows the results from the Numerical Optimization Pressure (NOP) case,

where the pressure at the outlet was set as a boundary condition. For both of the cases, a local minimum was found.

4.2.1 Error Analysis and Implementation Consistency

The numerical values of the consistency checks performed for the profiles resulting from numerical optimization are shown in Table 4.2 and Table 4.3. ODES is an abbreviation for ODE Solution and refers to the method of re-integrating the governing equations after optimization outlined in Section 3.3.1. This method of re-solving the governing equations with the optimal u profile reproduced the flow variable profiles resulting from numerical optimization for both NOR and NOP. Table 4.2

Numerical Optimization Radius (NOR) Case

Consistency Check	Quantity	Optimization Solution	ODES with Optimal u
Mass Balance	$\max\{D_m\}$	1.6×10^{-5}	1.4×10^{-17}
Energy Balance	$\max\{D_h\}$	2.1×10^{-5}	8.2×10^{-11}
Entropy Balance	Δs	0.0672 W/K	0.0656 W/K
Total Entropy Production	σ_{tot}	0.0657 W/K	0.0656 W/K
Relative Deviation	D_s	2.2 %	-4.5×10^{-4} %

Table 4.2: Numerical values for the consistency checks performed for the Numerical Optimization Radius (NOR) solution. The deviations used in the tables are $D_m = \dot{m}_i - \overline{\dot{m}}$, $D_h = h_{s,i} - \overline{h_s}$ and $D_s = (\Delta s - \sigma_{\text{tot}})/\Delta s \times 100\%$ as described in Section 3.3.1.

Numerical Optimization Pressure (NOP) Case

Consistency Check	Quantity	Optimization Solution	ODES with Optimal u
Mass Balance	$\max\{D_m\}$	1.6×10^{-5}	1.4×10^{-17}
Energy Balance	$\max\{D_h\}$	2.8×10^{-8}	8.1×10^{-11}
Entropy Balance	Δs	0.0703 W/K	0.0689 W/K
Total Entropy Production	σ_{tot}	0.0689 W/K	0.0689 W/K
Relative Deviation	D_s	2.0 %	-2.2×10^{-4} %

Table 4.3: Numerical values for the consistency check performed for the Numerical Optimization Pressure (NOP) solution. The deviations used in the tables are $D_m = \dot{m}_i - \overline{\dot{m}}$, $D_h = h_{s,i} - \overline{h_s}$ and $D_s = (\Delta s - \sigma_{\text{tot}})/\Delta s \times 100\%$ as described in Section 3.3.1.

and Table 4.3 show that mass and energy are conserved in both NOR and NOP solutions, with the errors being equal to zero to within machine precision for the re-integrated solution. The relative deviations between the entropy calculations in the middle column are high, and it is desired that the deviations are at least as low as in the right column to ensure consistent thermodynamics. The fairly large deviation prior to re-integration of the profile is attributed to errors because of the choice of discretization scheme combined with the equidistant grid used in the optimization. Increasing the

number of grid points by one order of magnitude reduced the error of D_s in the middle columns one order of magnitude, which indicates convergence.

It is observed that the solution obtained after integrating the optimal radius slope profile is more accurate than the solution obtained from optimization. As discussed in Chapter 3, this is because the minimization is performed over an equidistant grid, whereas the integrator used employs an adaptive step-size integration scheme, placing more grid points in the vicinity of high gradients. Because a relatively small amount of $N = 150$ grid points were used, the node spacing can affect the accuracy by a fair amount. The accuracy of the discretization scheme employed combined with the relatively coarse grid can definitely be criticized, but the choice was pragmatic and meant to ensure a stable solution.

The conclusion is that the solutions obtained are consistent with the model implementation, meaning that the local minima found for the two cases are solutions to the constrained optimization problem formulated for minimization of total entropy production in the pipe flow model.

4.2.2 Numerical Optimization Radius (NOR) Case

In Figure 4.4, the radius profile and its slope for the Numerical Optimization Radius (NOR) case solution are depicted. The profiles are very different from the constant linear radius profile of the typical ejector diffuser section used as a reference case. We observe an increase of the radius to a maximum value, before the radius decreases until it meets the boundary condition at the pipe outlet. The sharp turn makes this radius profile not appealing for practical applications where an expansion of the fluid is desired. This is because the goal of the expansion is to increase the pressure by lowering the velocity through momentum transfer. In a real, three-dimensional flow, a sharp turn would cause an unwanted momentum transfer to the wall because the flow will impinge on the wall and has to be turned away. This would also lead to swirling turbulent motions that would dissipate the energy of the flow.

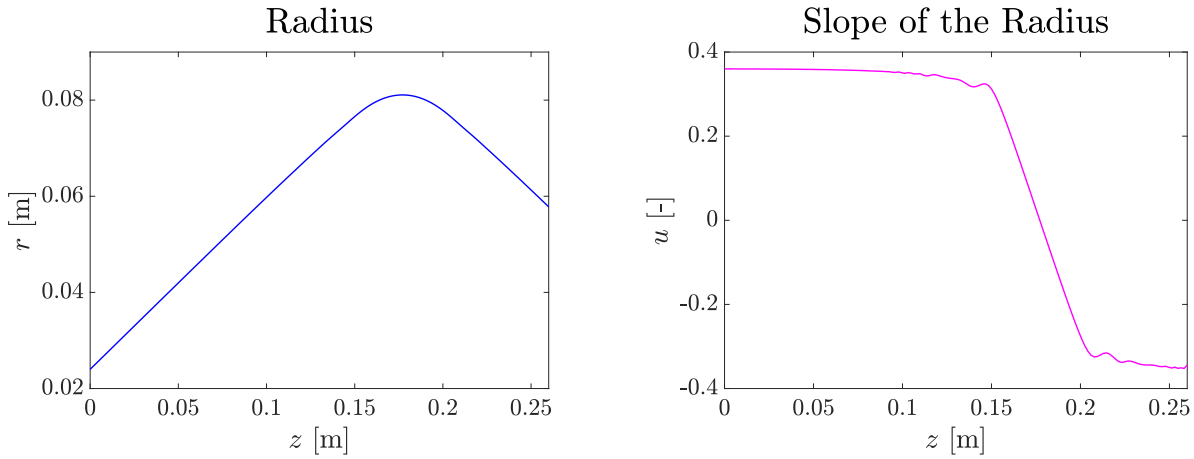

Figure 4.4: Profiles of the radius and its slope for the Numerical Optimization Radius (NOR) solution.

Additionally, the flow in the upper part of the pipe leaving along the steeply descending pipe wall would impede on the core of the flow, leading to momentum loss. The sharp edge at the outlet of the pipe may also cause separation of the flow, which would lead to extra momentum loss downstream of the outlet due to increased drag forces [51, 52]. If this diffuser section was used in for example an ejector there would most likely be a process component such as a compressor downstream of the outlet. The separation could cause inflow distortion to the compressor, lowering the performance of the thermodynamic cycle in which it is operating [45].

The slope of the radius profile at the inlet of the pipe is steeper than in the reference case, being equal to the value set as a numerical bound for u in the numerical solver. To repeat, these numerical bounds were the maximum values that a variable was allowed to attain at any grid point in the solution. The u value of almost 0.4 represents an angle equal to approximately 20°, which is a high value for a diffuser. Studies have shown that a diffuser angle of divergence equal in the range of $6-8°$ is optimal for a conical diffuser [44, 45]. The reference case (7.4° angle of divergence) lies within this range. The large angle of divergence could lead to separation of the flow. This separation would increase drag forces and increase entropy production in the flow.

An explanation for the profiles in Figure 4.4 is the following. We are minimizing the total entropy production which is solely due to friction forces. Because these friction forces increase with the square of the velocity and decrease for an increasing radius, we would want to expand the fluid quickly to obtain the lowest velocity possible throughout the whole pipe. This will be analyzed more theoretically in the next subsection.

It is observed that the slope of the radius is utilizing the maximum value of its numerical bound for as long as possible, before changing sign and taking the lower bound value. The slope profile is reminiscent of a step-function solution, which for a discontinuous step would yield a right-angled corner. A couple of small spikes in the slope of the radius are observed. These spikes smoothed out when the number of grid points was increased, indicating that the irregularities are due to numerical errors.

Theoretical Analysis of the Radius Profile Shape

A relation that can be used to analyze the radius profile shape theoretically was derived in Section 2.2.4. The following equation was established by setting the total entropy production σ_{tot} and the macroscopic entropy change Δs equal to each other:

$$\frac{\sigma_{\text{tot}}}{\dot{m}} = -R \ln \frac{P_f}{P_0} - \int_{z=0}^{z=L} \frac{d(\frac{V^2}{2})}{T}. \tag{4.1}$$

Here, the total entropy production is related to the pressure lift P_f/P_0 and a third therm which in a way represents the change in kinetic energy $V^2/2$ of the flow. Equation (4.1) can therefore almost be interpreted as the statement that minimum entropy production would be maximizing the pressure lift and change in kinetic energy simultaneously, at least for small variations in the temperature T. Considering only Equation (4.1), increasing the kinetic energy change is more effective than increasing the pressure lift, since a quadratic function grows considerably faster than the logarithmic function. However, we also need to regard the local entropy production

$$\sigma = \frac{\dot{m} f}{8} \frac{V^2}{TA} \frac{dS}{dz}. \tag{4.2}$$

This is where non-equilibrium thermodynamics serves its purpose. Equation (4.1) quantifies the total entropy production in terms of initial and final states of the system. Equation (4.2) quantifies the local irreversibilities, and therefore how to get from an initial to a final state efficiently. With minimization of the total entropy produced (Equation (4.1)) as a goal, Equation (4.2) is a tool that can aid us in finding out how we can do this efficiently, and in a way that is consistent with the physics of the system.

It is clear from the σ expression that, locally at a given axial coordinate, a low velocity is desired for low local entropy production. Because the flow is assumed to be adiabatic, a reduced velocity would increase the temperature. This would also reduce the local entropy production. Additionally, a larger area leads to less local entropy production. But there is a trade-off present in Equation (4.2), because increasing the area drastically would yield a large local change in surface area dS/dz which is a function of the slope u, which would increase the local entropy production.

Based on the above, the radius profile in Figure 4.7 resulting from optimization makes sense. The radius is increased at the start of the pipe to increase the area and lower the velocity, with both actions having the effect of reducing local entropy production. How rapidly this happens determines the magnitude of the local surface area change dS/dz, so there is a trade-off present in terms of how fast the area should change. Apparently, the slope is in this case not so large that dS/dz becomes unfavorably large for the local entropy production. Numerical experiments were conducted to check whether increasing the numerical bounds on the slope of the radius would continue to yield the same type of profiles. Figure 4.5 shows the radius profile and its slope when setting the numerical upper and lower bounds of u to 3 and -3, respectively. The profiles show that the maximum slope is utilized at the beginning of the pipe for this solution as well. Even though the slope of the radius is less like a step-function for this simulation, the local minimum found in this case is of the same nature as the one previously discussed, and even less applicable in practice.

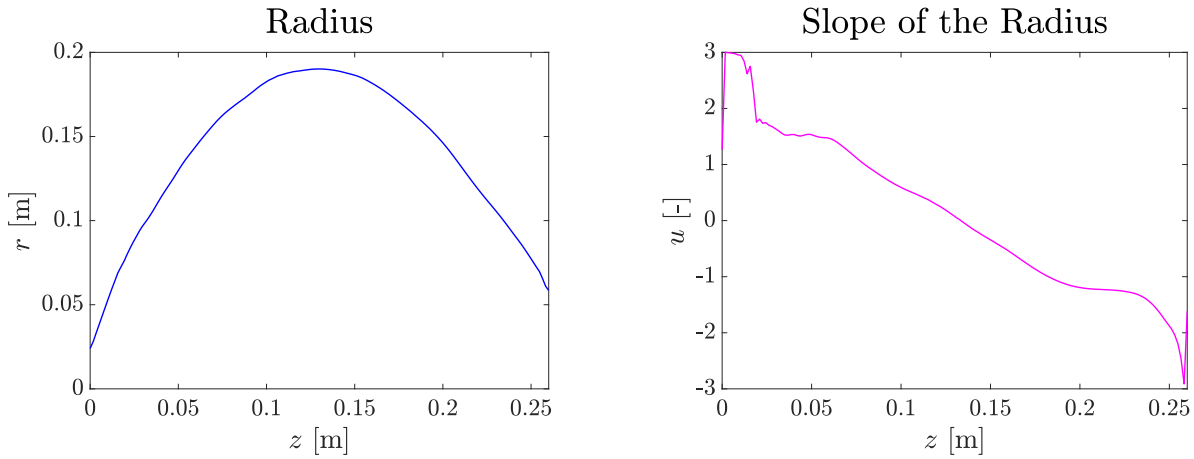

Figure 4.5: The radius profile and its slope for the Numerical Optimization Radius (NOR) case when increasing the numerical upper and lower bounds on the slope u to 3 and -3, respectively.

It is by now evident that the only reason the slope changes at one point is due to the radius boundary condition at the outlet of the pipe. Without numerical bounds on the slope of the radius and a radius boundary condition, the radius profile would be such that the fluid would be expanded to stagnation as fast as possible. It might not be the case that setting the outlet radius is the best choice of boundary condition for optimization, but it is clear by now that without any bounds on the slope and without a boundary condition at the outlet, the optimization problem would become completely meaningless. It is not completely trivial to set the boundary conditions for this model, however, as the one-dimensional flow model is prone to setting up an over-specified problem.

Local Entropy Production and Flow Variable Profiles (NOR)

The resulting entropy production profile of the NOR solution is presented in Figure 4.6. In the left figure, it could seem like the local entropy production is approximately equipartitioned (constant) in the right half of of the pipe. This could be a sign of parts of the system attaining a state of equipartitioning of entropy production. Johannessen [3] observe that for some efficient process equipment solutions, the entropy production may not be equipartitioned in the entire system, but small subsections of the system will exhibit constant entropy production. However, the enlarged view of the portion of the pipe with seemingly constant entropy production shown in the right part of the figure shows that this is not the case here.

For the NOR solution, the total entropy production was 0.0656 W/K, which was an immense

reduction of 60% compared to the reference case. This is far more than what has been accomplished in other studies where optimization of energy processes based on minimization of entropy production was performed [8–11]. The reduction potential of 60% is considered unrealistic, due to the detrimental effects the radius profile shape would have on the flow that were discussed earlier. It is expected that this large value would not be obtained if the complexity of the physical model was higher, such that the flow features mentioned earlier could be accounted for. Future studies should look into this in more detail; an analysis similar to the present work for a planar, laminar flow could for example be a great start, since this would add two-dimensional flow features to the analysis without overly complicating the mathematics.

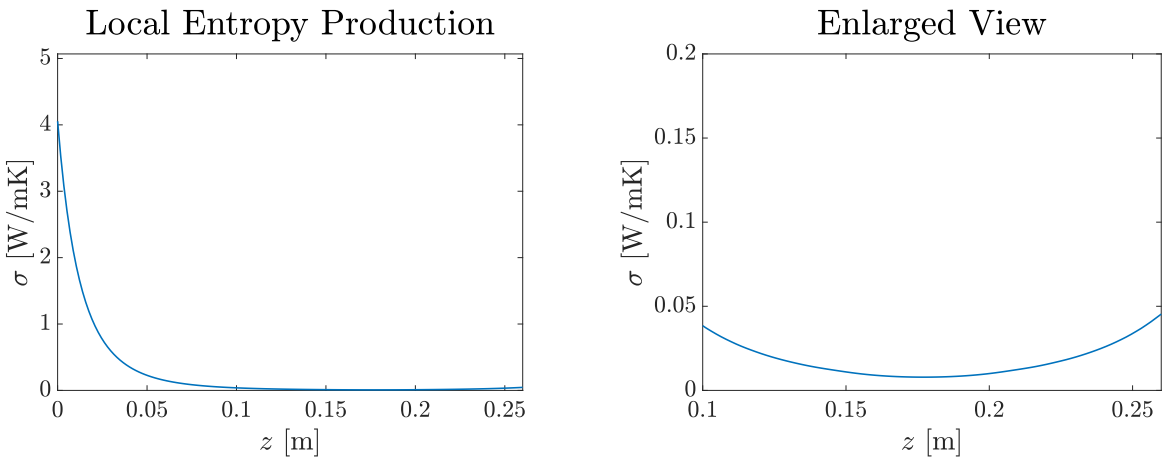

Figure 4.6: Local entropy production in the pipe calculated with the variable profiles for the Numerical Optimization Radius (NOR) case. To the right is an enlarged view of the profile in the area where it seems constant in the left figure.

The flow variable profiles for the NOR solution are presented in Figure 4.7. The velocity profile for NOR decreases more rapidly than the velocity profile in the reference case. This is because of the favorable effect this has on the local entropy production, as discussed earlier. The outlet pressure for the NOR solution was higher than for the reference case, which follows from a decrease in the total entropy production and thus less friction loss. A slight decrease in the velocity at the outlet when compared to the reference case is observed. For a diffuser where the highest possible outlet pressure is of interest, this is a favorable pressure-velocity trade-off. In an application where the magnitude of the velocity of the fluid at the outlet is important, however, one would have to consider the trade-off between the two differently.

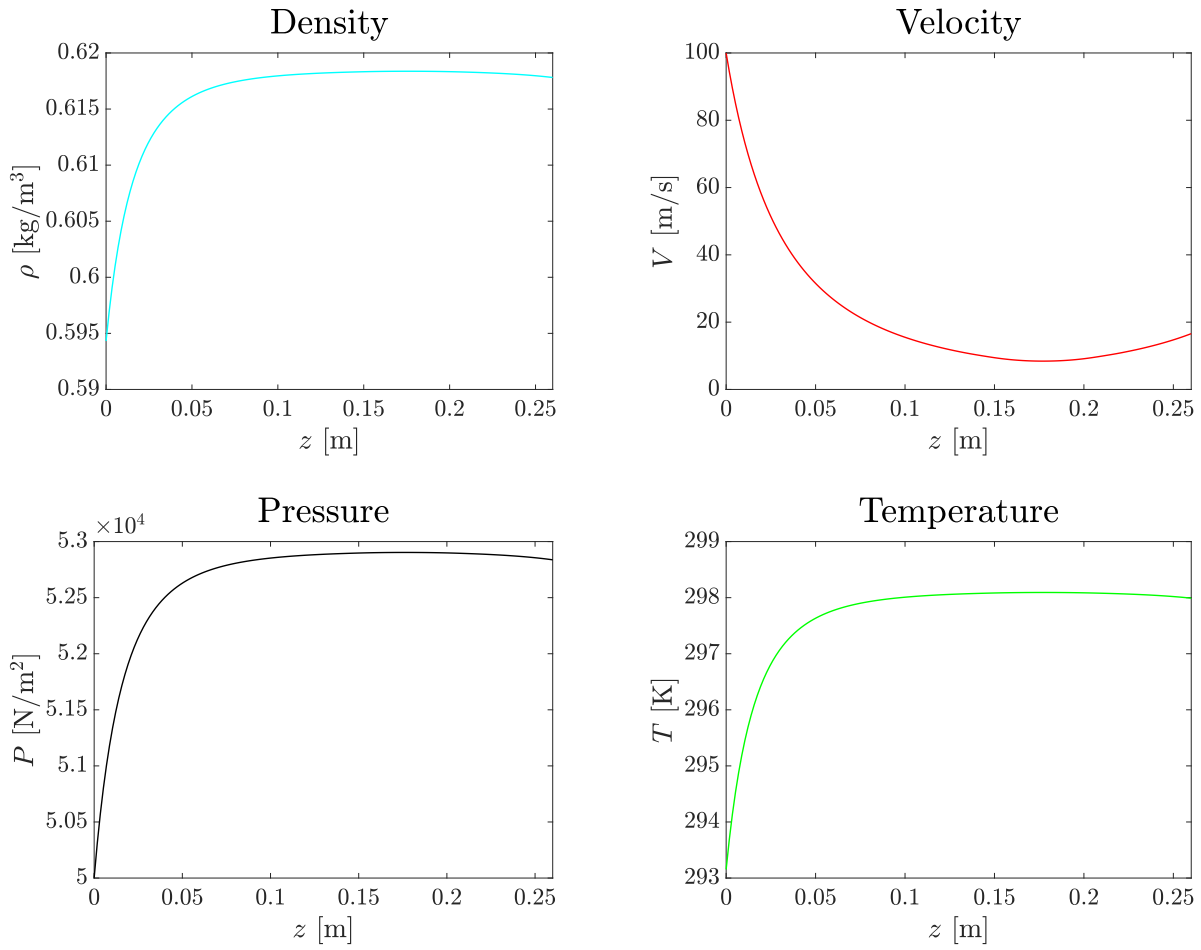

Figure 4.7: Profiles of the flow variables for the Numerical Optimization Radius (NOR) solution.

4.2.3 Numerical Optimization Pressure (NOP) Case

The profiles of the radius and its slope for the Numerical Optimization Pressure (NOP) case solution are depicted in Figure 4.8. We observe similar profiles to the ones for NOR, with the sharp turn being more pronounced in this case. This makes the NOP slope profile even more similar to a step-function than for the profile in NOR. The point where the slope changes sign is slightly earlier in the pipe for NOP when compared to the NOR solution. For NOP, the outlet radius was free to vary. The resulting outlet radius for NOP was lower than the outlet radius in the reference case and NOR. For NOP, the outlet radius $r_f = 0.0443$ m compared to the outlet radius $r_{f,\text{ref}} = 0.0578$ m.

Obtaining the same type of radius profile in NOP as in NOR indicates that the same type of local minimum has been found, where velocity is reduced quickly to reduce the local entropy production. Therefore, the discussion of the radius profile's effects on the flow and practical considerations carried out in Section 4.2.2 also apply here. The effect on the flow in terms of wall impingement would be stronger for NOP, since the turn is sharper than for the NOR solution.

Local Entropy Production and Flow Variable Profiles (NOP)

The local entropy production profile for NOP is depicted to the left in Figure 4.9. To the right is an enlarged view of the middle section of the pipe. For this case, the total entropy production was 0.0689 W/K. This is slightly higher than in NOR, but still almost a 60% decrease from the reference

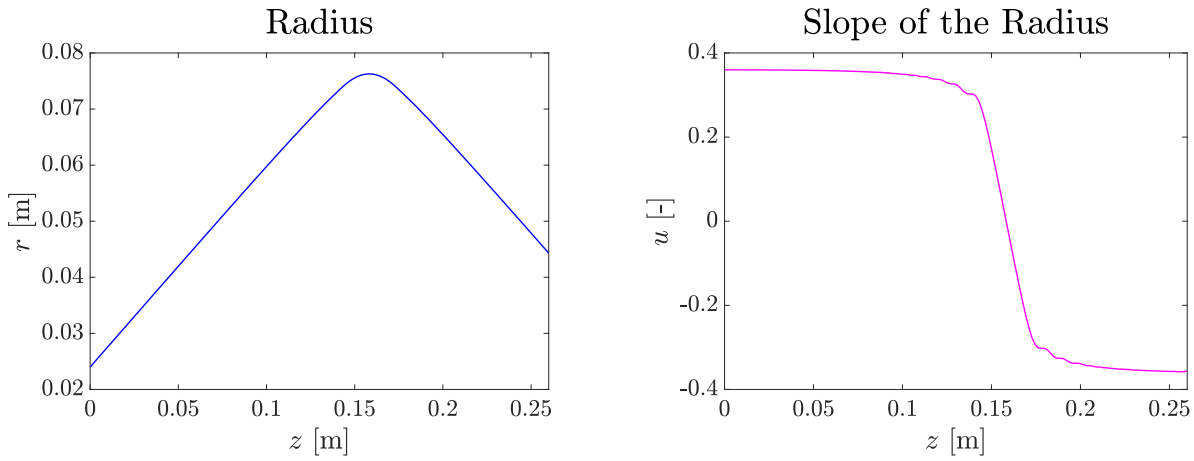

Figure 4.8: Profiles of the radius and its slope for the Numerical Optimization Pressure (NOP) solution.

case. Since the NOP radius profile is similar to the NOR solution, this reduction potential is also considered unrealistic. The region where the profile to the left in Figure 4.9 seems constant shown with an enlarged view to the right, proving that no local equipartitioning of entropy production is observed for this case either. The fact that none of the local entropy production profiles obtained with numerical optimization are equipartitioned may imply that the local minima found are not global solutions. Because equipartitioning in earlier works has been shown to either be the state of minimum entropy production [6, 7], or at least a good approximation to the state of minimum [3, 8, 9], we should expect to find a local entropy production profile which is more constant if it were in fact the global minimum.

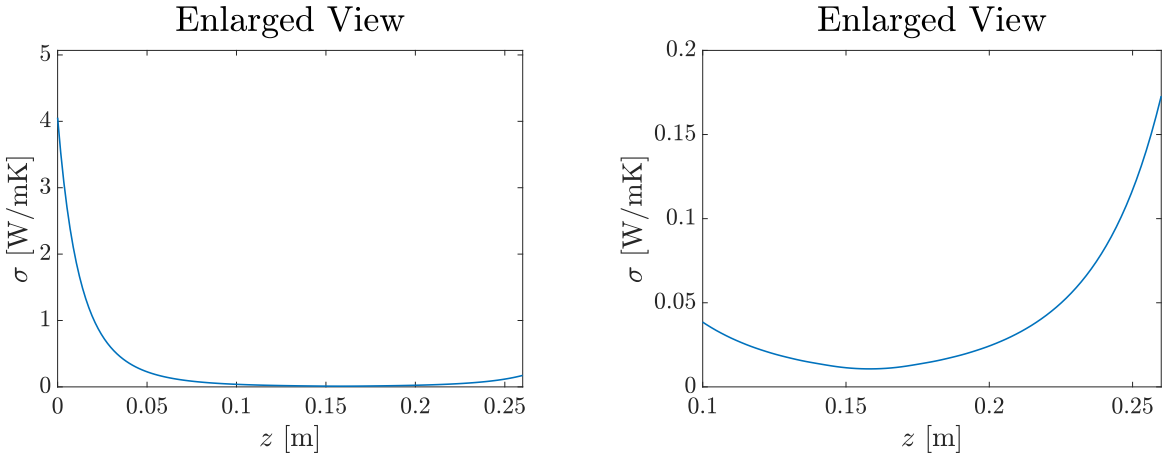

Figure 4.9: Local entropy production in the pipe calculated with the variable profiles for the Numerical Optimization Pressure (NOP) solution. To the right is an enlarged view of the profile in the area where it seems constant in the left figure.

The flow variable profiles obtained for NOP are shown in Figure 4.10. Compared to NOR and the reference case, the outlet velocity is now greater. The outlet value $V_f = 28.3$ m/s is almost double the value of the NOR outlet velocity, which was 16.6 m/s. This is consistent with the total entropy

production expression in Equation (4.1), repeated here for clarity:

$$\frac{\sigma_{\text{tot}}}{\dot{m}} = -R \ln \frac{P_f}{P_0} - \int_{z=0}^{z=L} \frac{d(\frac{V^2}{2})}{T}. \tag{4.3}$$

Because the outlet pressure P_f is set for NOP, and the inlet variables are set, minimization of the total entropy production now constitutes maximization of the second term on the right-hand side of Equation (4.3), which results in a larger difference between the inlet and outlet velocity for the NOP case when compared to NOR and the reference case. Equation (4.3) approximately constitutes maximization of outlet velocity for low temperature variations. Equation (4.3) puts a bound on the change of the velocity term, though, because the Second Law of Thermodynamics requires that

$$\sigma_{\text{tot}} \geq 0.$$

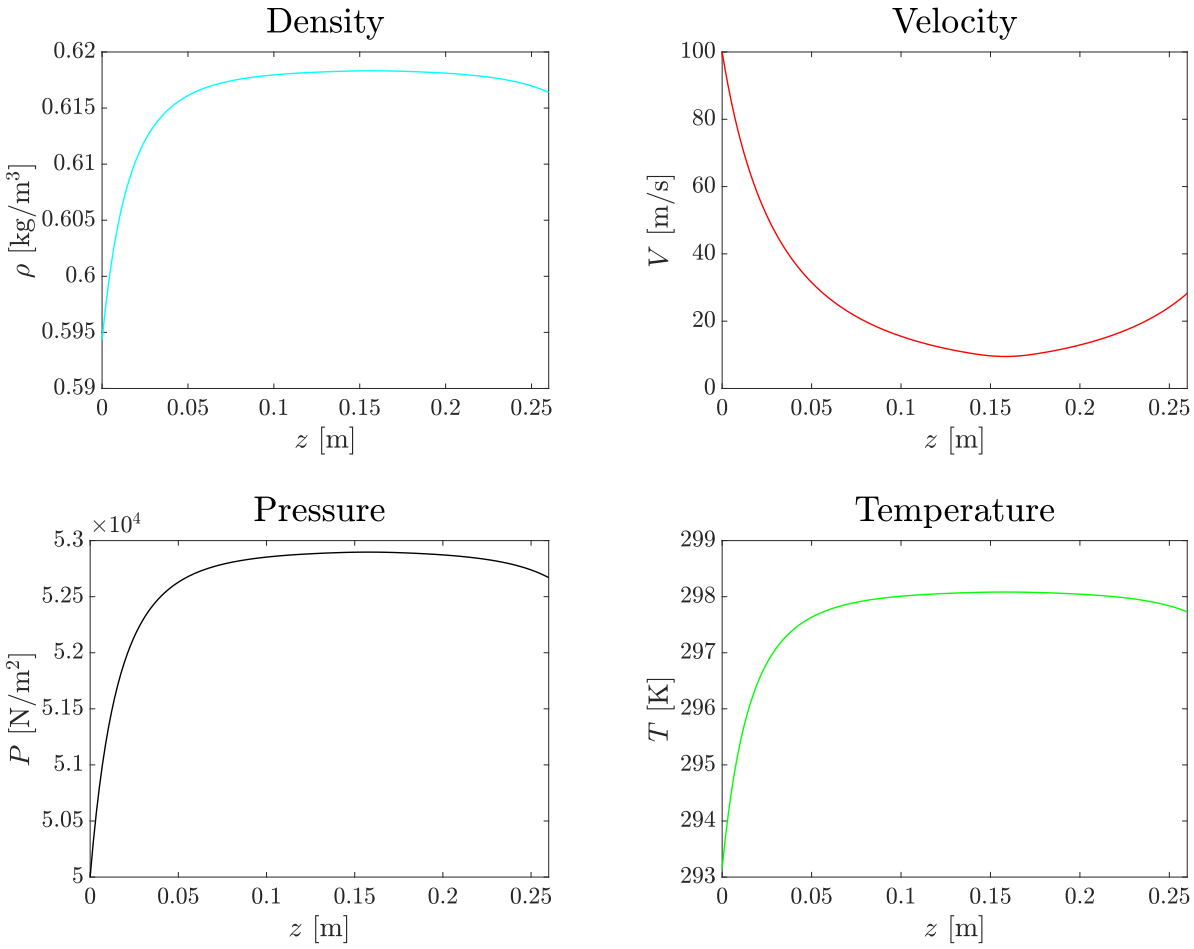

Figure 4.10: Profiles of the flow variables for the Numerical Optimization Pressure (NOP) solution.

4.2.4 Model Limitations and Future Work

To investigate other types of solutions than the local minimum found with numerical optimization in this work, it is evident that more physics needs to be added to the model. Johannessen [3] performed optimization of a plug flow reactor, which was a flow model similar to the one used in this work

but with more physical mechanisms present. There, irreversibilities due to both pressure drop, heat transfer and chemical reactions were accounted for, and great results were obtained. Inspired by this, adding for example heat transfer to the fluid through the pipe wall to the model used in this work could be a thing to investigate in future work. This would result in a trade-off mechanism between the local entropy production due to friction and the local entropy production due to heat transfer, which could yield more interesting radius profile solutions.

Based on the discussions in Section 4.2.2 and Section 4.2.3, it is clear that numerical bounds are very decisive for the results in the optimization. If further work is done on this type of numerical optimization of radius profiles in pipe flow, a convenient way of constraining the type of solution could be to set a constraint for the maximum surface area of the pipe. This would prevent the type of local minima found in the present work.

Another thing which could affect the type of solution obtained are the boundary conditions set for the two cases. Future work should investigate whether different combinations of boundary conditions can lead to more meaningful solutions in the practical sense. However, as mentioned previously, it is easy for a simple model as the one considered in this work to over-specify the problem. It might therefore be easier to set the boundary conditions for a model where more physical mechanisms are included.

In the numerical constrained optimization implementation in this work, derivatives were discretized with the upwind scheme and midpoint values of the variables were used. This can lead to inaccurate representation of the physics of the problem, because the variable values and their changes are not perfectly related. Additionally, the upwind scheme is a low-order-of-accuracy discretization scheme. Future studies could investigate using more accurate methods.

The discussion of the numerical optimization is incomplete without addressing the limitations of the model implemented. One aspect of the radius profile obtained from optimization discussed previously is the impact resulting two- and three-dimensional flow features would have on the flow, which are not accounted for with the cross-sectional averaged one-dimensional model used here. Another limitation with the model is the assumption of steady state. This can in general be valid for process equipment operating in a thermodynamic cycle where the operating state is constant. Interestingly, Ornano *et al.* [53] found that for a nozzle used in a hydrogen-air detonation combustor, the optimal shape of the radius profile of the nozzle differed for the two cases of steady and unsteady flow. This indicates that the resulting radius profile could be different if transient flow was analyzed.

The velocity profile could take a different shape if the friction factor was not held constant, but instead was a function of the Reynolds number of the flow and the diameter of the pipe, which is the general case for pipe flow. For very high Reynolds numbers, a type of roughness-independence has been observed in experiments, such that changes in the Reynolds number do not affect the friction factor significantly and it remains approximately constant [42]. For ejectors, this flow regime is often the case. If the flow was in a transitional regime between turbulent and laminar flow, however, significant changes to the friction factor would occur when the velocity of the flow slowed down, altering the dynamics of the problem. This is relevant for many applications of pipe flow and viscous flow in confined geometries [32]. Moreover, the friction factor depends on what is defined as a relative roughness ϵ/D, where ϵ is the roughness of the pipe material and D is the pipe diameter. Increasing the diameter of the pipe decreases the magnitude of the friction forces. To summarize, a decent amount of the fluid dynamics of the problem is neglected when the friction factor is assumed to be a constant. Future work should therefore investigate the effects of using a varying friction factor on the numerical optimization solution.

To conclude, even though local minima were found for both the Numerical Optimization Radius (NOR) case and the Numerical Optimization Pressure (NOP) case, the numerical optimization results cannot be characterized as optimal radius profiles for pipe flow or diffuser applications. The entropy production reduction potential observed for the radius profiles of both NOR and NOP are considered

unrealistic, because the profiles would lead to detrimental flow phenomena. However, the results show that variations in the radius profile can reduce total entropy production, providing hope for future work on the topic.

4.3 Optimal Control Theory

The results of optimization performed with optimal control theory are presented here. A solution to the problem formulated was unfortunately not successful. The iterative solver used gave results for the radius boundary condition optimization case that proved to not be a solution of the optimization problem, and the errors of the result are discussed. Possible explanations for why the solution of the problem was unsuccessful are discussed and the error analysis performed to investigate the source of problem is covered.

The iterative solver used to solve the two-point boundary value problem (BVP) of the optimal control theory formulation returned a result for the radius boundary condition case. However, calculation of the Hamiltonian of the results show that the result is not a solution to the optimization problem, see Figure 4.11. As discussed earlier, the Hamiltonian of the problem is autonomous and should therefore be constant throughout the system for an optimal state, which it clearly is not.

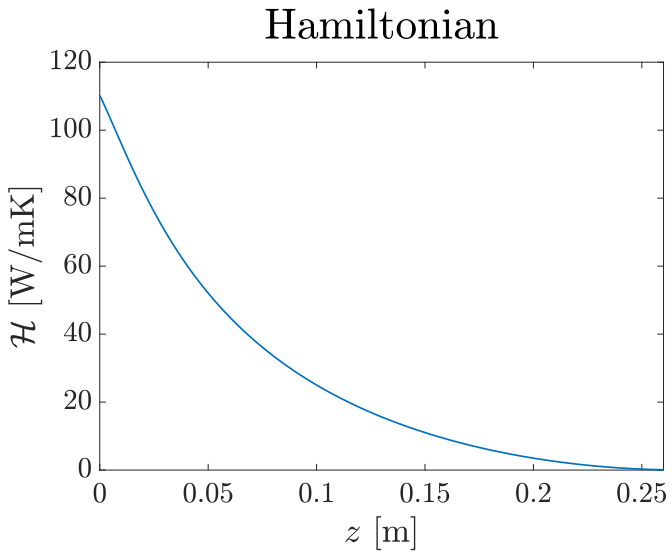

Figure 4.11: The Hamiltonian of the problem for the result returned by the iterative solver used for the optimal control theory optimization problem formulation.

To investigate the source of the problem with the optimal control theory problem formulation and implementation, the first thing done was to perform consistency checking of the solution. The results are shown in Table 4.4. We observe that the physics of the results are consistent with the model implemented. Supported by the consistent results in Section 4.1 and Section 4.2, it was concluded that the implementation of the fluid dynamic model and the local entropy production was not the source of error. Just to display what type of result was returned by the iterative solver used, the radius profile and its slope are depicted in Figure 4.12. Since the Hamiltonian showed that this is not a solution, the resulting radius profile is considered just a coincidence. It is noted that the total entropy production is 45% less than for the reference case. Because the result obtained is not a solution, a discussion of the flow variable profiles and the entropy production profiles is deemed invaluable and will not be carried out. The only thing that will be noted is that no equipartitioning of the local entropy production was observed for this radius profile either, which is expected since it is not a solution to the minimization problem.

Let us now continue studying the possible sources of error in the problem formulation and implementation. With the optimal control theory being a comprehensive problem formulation, there are several things that may be the source of error in the problem formulation or derivation. Knowing

Optimal Control Theory: Radius Boundary Condition Case

Consistency Check	Quantity	BVP Solver Result	ODES with Resulting u
Mass Balance	$\max\{D_m\}$	1.6×10^{-5}	1.4×10^{-17}
Energy Balance	$\max\{D_h\}$	2.8×10^{-8}	8.1×10^{-11}
Entropy Balance	Δs	0.0923	0.0902
Total Entropy Production	σ_{tot}	0.0904	0.0902
Relative Deviation	D_s	2.1 %	1.4×10^{-6} %

Table 4.4: Numerical values for the consistency check performed for the result returned by the iterative solver used for the optimal control theory optimization problem formulation. The deviations used in the tables are $D_m = \dot{m}_i - \overline{\dot{m}}$, $D_h = h_{s,i} - \overline{h_s}$ and $D_s = (\Delta s - \sigma_{\text{tot}})/\Delta s \times 100\%$ as described in Section 3.3.1

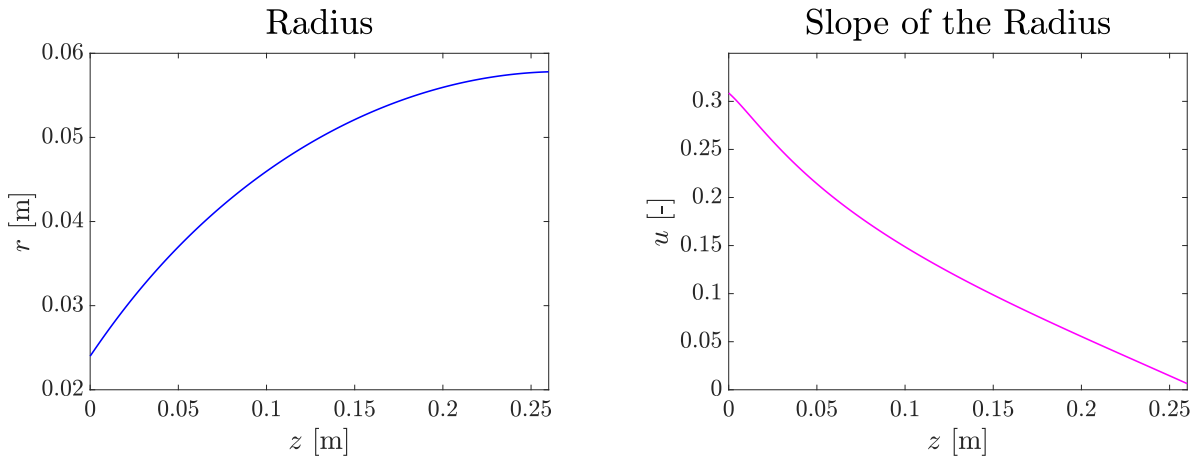

Figure 4.12: Profiles of the radius and its slope for the result returned by the iterative solver used for the optimal control theory optimization problem formulation.

that the fluid dynamic model and the local entropy production were correctly implemented, checking the correctness of the partial derivatives of the Hamiltonian was a natural next step. Correctness in these partial derivatives are paramount to the problem since they yield both the algebraic equation for the control variable and the governing equations of the multiplier functions. Checking of these derivatives was done by checking the error between the analytical partial derivatives and a central difference calculated with a relative perturbation of the variable being differentiated with respect to. The method was outlined in Section 3.3.2. Numerical results of the perturbation analysis are given in Table 4.5. We observe small orders of magnitude in the errors, which should indicate that the partial derivative expressions derived are correct. The maximum error of $\partial\mathcal{H}/\partial u$ is several orders of magnitudes lower than the other two, though, which may imply that small errors have been made in the partial differentiation. Because of the implicit dependencies between the variables $\dot{M}$ and r used to construct the Hamiltonian and the flow variables ρ, V, P and T, there might be subtle mistakes that were made in the partial differentiation despite the numerical results presented in Table 4.5. This could explain why the error of $\partial\mathcal{H}/\partial u$ is much lower than the other two.

The approach used in Section 2.3.3 of dealing with the dependencies between r and ρ and P by calculating $\partial P/\partial r$ and $\partial\rho/\partial r$ such that $\partial\dot{M}/\partial r$ was equal to zero was only applied at a late stage in

Partial Derivative	Max Error	Mean Error	Standard Deviation
$\frac{\partial \mathcal{H}}{\partial u}$	1.7×10^{-9}	-1.6×10^{-10}	1.1×10^{-9}
$\frac{\partial \mathcal{H}}{\partial \dot{M}}$	1.4×10^{-5}	-6.8×10^{-9}	1.7×10^{-6}
$\frac{\partial \mathcal{H}}{\partial r}$	3.4×10^{-5}	4.4×10^{-7}	2.7×10^{-5}

Table 4.5: Numerical results of the consistency checks performed for the partial derivatives of the Hamiltonian.

this work. The author now begs the question whether dependencies should also have been taken care of to ensure that $\partial r/\partial \dot{M}$ is also equal to zero, since the momentum flow rate $\dot{M} = A\left(P + \rho V^2\right) = \pi r^2 \left(P + \rho V^2\right)$ clearly mathematically speaking depends on r. It was however thought that r was supposed to be uniquely determined by the control variable $u = dr/dz$, since r follows from integration of u. The lack of correctly accounting for dependencies, whether that is wrongly calculated partial derivatives or lacking partial derivative calculations, are both highly likely to be the source of error. Not only do are they important for the BVP formulated, but they also affect the boundary conditions derived with the transversality condition in Section 3.2.1. This incorrect handling of the boundary conditions could then also be the source of error. These variable dependencies should therefore be investigated in future work.

An alternative approach would be to not reformulate the governing equations such that one integrates $\dot{M}$, but rather use the more normal approach of formulating ODEs for all of the variables ρ, V, P, T. This was briefly attempted in the present work. This results in five ODEs for the variables ρ, V, P, T and r, and the resulting Hamiltonian $\mathcal{H}_a$ for this alternative approach would be

$$\mathcal{H}_a = \sigma + \lambda_1 \frac{d\rho}{dz} + \lambda_2 \frac{dV}{dz} + \lambda_3 \frac{dP}{dz} + \lambda_4 \frac{dT}{dz} + \lambda_5 \frac{dr}{dz}.$$

With the same choice of control variable $u = dr/dz$, the resulting necessary conditions for an optimal trajectory is a two-point boundary value problem of ten differential equations with this approach because there are now five variables and five multiplier functions. The partial differentiation required to derive the necessary conditions was practically impossible to perform by hand. Therefore, symbolic differentiation in MATLAB with *syms* [54] was performed. This solution attempt resulted in problems with solving the algebraic equation $\partial \mathcal{H}/\partial u = 0$, and because of both the complexity and lack of transparency in this approach, this problem setup was not further pursued.

There exists the possibility that no solution to the problem exists with the present formulation. The possibility of this is assumed to be very small, however. It is expected that a solution should exist for such a (relatively) simple system. Failure to find a solution to the problem could also be because the initial guess provided to the solver is not good enough. The solutions to boundary value problems with the collocation may depend heavily on the initial guess. A possible explanation could therefore be that the initial profile guesses prevent the solver from converging to a correct solution. However, since the necessary conditions derived for a minimum should ensure a stationary state for the Hamiltonian, errors in the derivation of the necessary conditions or the implementation are much more plausible explanations for the unsuccessful solution rather than problems with solution existence.

Another aspect of the problem formulation which could potentially lead to problems with finding

a solution is the nature of the stationarity condition

$$\frac{\partial \mathcal{H}}{\partial u} = \frac{\dot{m} f V^2}{4rT} \frac{u}{\sqrt{1+u^2}} + \lambda_1 \left(2\pi r P - \frac{\dot{m} f V}{4r} \frac{u}{\sqrt{1+u^2}} \right) + \lambda_2 = 0, \tag{4.4}$$

which we want to solve for the optimal control u. Problems with the solution of this equation in terms of u were briefly pointed out in Section 2.3.3. Because of the appearance of both square-root expressions and u^2, existence and uniqueness of the solution to Equation (4.4) might give rise to complications. In fact, solving this equation was the first approach attempted in this work. The use of

$$u = -\frac{2\pi r P \lambda_1 + \lambda_2}{\mathcal{H}}$$

was only developed later on, motivated by the need for a different way of finding the optimal u than solving Equation (4.4) directly.

Notwithstanding the failure of correctly solving the optimal control theory problem formulated, it can hopefully be either directly used in or at least inspire future work on the topic.

Chapter 5

Conclusion

Fluid flow and thermodynamic irreversibilities served as motivation for the development of a one-dimensional model of adiabatic, viscous, single-phase flow of air modeled as an ideal gas in a pipe of varying cross section in this work. An expression for the local entropy production of the flow was derived. A constrained optimization problem was defined with the total entropy production of the flow as the objective function to be minimized. Additionally, an optimization problem using optimal control theory was formulated. The fluid dynamic model and the optimization routines were implemented and the problems were solved numerically. Results of the optimization were compared with a reference case, which constituted flow in a pipe with a linear radius profile increasing in radius from inlet to outlet. This reference case was motivated by the diffuser section of a typical air ejector. Two optimization cases were analyzed; one where the outlet radius was set, the other where the outlet pressure was set. For both optimization cases, all inlet boundary conditions were equal to the values of the reference case. To ensure conservation of mass and energy and thermodynamic consistency, consistency checks and error analyses of the numerical results were carried out.

Results of the numerical constrained optimization suggest that alterations of the radius profile can reduce the entropy production of the flow. Compared to a reference case, a 60% reduction in the total entropy production was achieved by alteration of the radius profile. This reduction potential is not characterized as practically realizable, however, because the radius profiles obtained are not applicable to pipe flow. The reason for this is that the profile shape obtained would for a real, three-dimensional flow cause detrimental flow features that lead to undesired momentum losses. Among these flow features, wall impingement and separation of the flow would be the two most pronounced, causing momentum transfer to the wall and increased drag forces, respectively. Nevertheless, the profiles indicated that there exists potential for reduction in the total entropy production of the flow by variations in the radius profile.

The profiles obtained from numerical optimization were similar for the two optimization cases Numerical Optimization Radius and Numerical Optimization Pressure considered, and both solutions obtained satisfied the consistency checks performed. Therefore, the radius profiles found are a local minimum to the optimization problem formulated, and the lack of applicability of the profiles is due to model limitations. An explanation of the profile shapes was suggested, based on the reasoning that the fluid should attain the lowest velocity possible throughout the pipe to minimize the friction loss, since the local entropy production of the flow varied with the square of the velocity.

Further work on the numerical optimization performed here should consider adding more physics to the fluid dynamic model developed here. Based on the numerical optimization results, only accounting for friction losses leads to a local solution which is not of interest. Adding for example heat transfer to the model could create a trade-off mechanism between the local entropy production of the two mechanisms, potentially leading to radius profiles more interesting for practical applications.

In addition to the numerical constrained optimization, an optimal control theory optimization

problem was formulated and implemented. The solution of the problem was unsuccessful. For the radius boundary condition optimization case a set of profiles was produced by the iterative solver used. The Hamiltonian of the solution was not a constant, which it should have been for the problem formulated, proving that the result was not a solution to the optimization problem. It is noted that the resulting radius profile reduced total entropy production by 45% compared to the reference case.

There are several possible explanations as to why the optimal control theory approach failed to yield a solution. Error analysis of the implementation and the solution procedure was done. Most likely, the dependencies of the variables in the problem formulation and the boundary conditions in the model implementation were not correctly handled. Not correctly accounting for the dependencies leads to erroneous partial derivatives of the Hamiltonian, which in turn leads to errors in the necessary conditions for a minimum. The dependencies and the derivatives also affect the boundary conditions resulting from the transversality condition. Both the choice of dependent variables and choice of boundary conditions should therefore be re-considered in future work.

To conclude, the fluid dynamic model developed here is too simple to provide optimized radius profiles with constrained numerical optimization that can be employed in practical applications of pipe flow. Hopefully, the optimal control theory work done here can serve as a reference for further work on the topic. Notwithstanding the problems with finding solutions in this work, first steps have been taken in the direction of finding the optimal radius profile of fluid flow in confined geometries, as the present work has demonstrated that variations in the shape of the radius profile of a pipe can reduce the total entropy production of the flow. With the topic of this thesis being a hitherto rather unexplored area of research in process engineering, the author hopes that the results of this work, despite their shortcomings, can help and inspire future work on geometric optimization of viscous flow in confined geometries with entropy production minimization.

Bibliography

[1] U.S. Energy Information Administration, *International Energy Outlook 2016*.

[2] S. Kjelstrup, D. Bedeaux, E. Johannessen, and J. Gross, *Non-Equilibrium Thermodynamics for Engineers*, 2nd. World Scientific, 2017.

[3] E. Johannessen, *The state of minimum entropy production in an optimally controlled system*, eng, Trondheim, 2004.

[4] A. Bejan, *Entropy generation minimization. The method of thermodynamic optimization of finite-size systems and finite-time processe*. New York: CRC Press, 1996.

[5] M. J. Moran, H. N. Shapiro, D. D. Boettner, and M. B. Bailey, *Fundamentals of Engineering Thermodynamics*, 8th. Wiley, 2014.

[6] D. Tondeur and E. T. Kvaalen, "Equipartition of entropy production. an optimality criterion for transfer and separation processes," 1987.

[7] D. Bedeaux, F. Standaert, K. Hemmes, and S. Kjelstrup, "Optimization of Processes by Equipartition," vol. 24, no. 3, pp. 242–259, 1999.

[8] E. Magnanelli, E. Johannessen, and S. Kjelstrup, "Entropy Production Minimization as Design Principle for Membrane Systems: Comparing Equipartition Results to Numerical Optima," *Industrial & Engineering Chemistry Research*, vol. 56, pp. 4856–4866, 2017.

[9] R. Hånde and Ø. Wilhelmsen, "Minimum entropy generation in a heat exchanger in the cryogenic part of the hydrogen liquefaction process: On the validity of equipartition and disappearance of the highway," *International Journal of Hydrogen Energy*, vol. 44, no. 29, pp. 15 045–15 055, 2019, ISSN: 0360-3199.

[10] E. Johannessen and S. Kjelstrup, "Minimum entropy production rate in plug flow reactors: An optimal control problem solved for so2 oxidation," *Energy*, vol. 29, no. 12, pp. 2403–2423, 2004, ISSN: 0360-5442.

[11] E. Magnanelli, S. B. B. Solberg, and S. Kjelstrup, "Nature-inspired geometrical design of a chemical reactor," *Chemical Engineering Research and Design*, vol. 152, pp. 20–29, 2019, ISSN: 0263-8762.

[12] "Solar ejector cooling systems: A review," *Renewable Energy*, vol. 164, pp. 566–602, 2021, ISSN: 0960-1481.

[13] S. Riffat, L. Jiang, and G. Gan, "Recent development in ejector technology - A review," *International Journal of Ambient Energy*, vol. 26, Mar. 2011.

[14] H.-S. Lee, J.-I. Yoon, C.-H. Son, S.-J. Ha, S.-H. Seol, B. Ye, H.-J. Kim, and G. J. Jung, "Efficiency enhancement of the ocean thermal energy conversion system with a vapor-vapor ejector," *Advances in Mechanical Engineering*, vol. 7, Mar. 2015.

[15] B. Vogel, "Energieeffizienter und günstiger dank Ejektor," *Alimenta*, Nov. 2017.

[16] E. Milner, *CO2 efficiency equator moves further south by grace of ejector technology*, Mar. 2015. [Online]. Available: `http://www.r744.com/articles/6235/span_style_color_rgb_255_0_0_update_span_co_sub_2_sub_efficiency_equator_moves_further_south_by_grace_of_ejector_technology`.

[17] S. Elbel and N. Lawrence, "Review of recent developments in advanced ejector technology," *International Journal of Refrigeration*, vol. 62, pp. 1–18, 2016, ISSN: 0140-7007.

[18] S. Elbel, "Historical and present developments of ejector refrigeration systems with emphasis on transcritical carbon dioxide air-conditioning applications," *International Journal of Refrigeration*, vol. 34, no. 7, pp. 1545–1561, 2011, Ejector Technology, ISSN: 0140-7007.

[19] T. S. Ltd. "Principle of Operation of Ejectors." (2020), [Online]. Available: `https://www.transvac.co.uk/how-an-ejector-works/`. (Accessed: 20.03.2022).

[20] Ø. Wilhelmsen, A. Aasen, K. Banasiak, and A. Hafner, "One-dimensional mathematical modelling of two-phase ejectors for expansion work recovery: Extension to mixtures and mapping of the local exergy destruction," unpublished.

[21] A. Arbel, A. Shklyar, D. Hershgal, M. Barak, and M. Sokolov, "Ejector Irreversibility Characteristics," *Journal of Fluids Engineering*, vol. 125, Jan. 2003.

[22] K. Banasiak, M. Palacz, A. Hafner, Z. Buliński, J. Smołka, A. J. Nowak, and A. Fic, "A CFD-based investigation of the energy performance of two-phase R744 ejectors to recover the expansion work in refrigeration systems: An irreversibility analysis," *International Journal of Refrigeration*, vol. 40, pp. 328–337, 2014, ISSN: 0140-7007.

[23] M. Nakagawa, T. Matumi, H. Takeuchi, and N. Kokubo, "Mixing of the confined jet of mist flow," *JSME international journal. Series B, fluids and thermal engineering*, 1996, ISSN: 1340-8054.

[24] K. Banasiak, A. Hafner, and T. Andresen, "Experimental and numerical investigation of the influence of the two-phase ejector geometry on the performance of the R744 heat pump," *International Journal of Refrigeration*, vol. 35, no. 6, pp. 1617–1625, 2012, ISSN: 0140-7007.

[25] S. Elbel and P. Hrnjak, "Experimental validation of a prototype ejector designed to reduce throttling losses encountered in transcritical R744 system operation," *International Journal of Refrigeration*, vol. 31, no. 3, pp. 411–422, 2008, ISSN: 0140-7007.

[26] A. Sahin, "A second law comparison for optimum shape of duct subjected to constant wall temperature and laminar flow," *Heat and Mass Transfer*, vol. 33, pp. 425–430, Apr. 1998.

[27] F. Kock and H. Herwig, "Local entropy production in turbulent shear flows: A high-Reynolds number model with wall functions," *International Journal of Heat and Mass Transfer*, vol. 47, pp. 2205–2215, May 2004.

[28] R. Pal, "Entropy Production in Pipeline Flow of Dispersions of Water in Oil," *Entropy*, vol. 16, pp. 4648–4661, Aug. 2014.

[29] A. Sahin and R. Ben-Mansour, "Entropy Generation in Laminar Fluid Flow through a Circular Pipe," *Entropy: International and Interdisciplinary Journal of Entropy and Information Studies*, vol. 5, Dec. 2003.

[30] I. Alzaharnah, "Entropy Analysis in Pipe Flow Subjected to External Heating," *Entropy: International and Interdisciplinary Journal of Entropy and Information Studies*, vol. 5, Dec. 2003.

[31] H. A. Jakobsen, *Chemical Reactor Modeling - Multiphase Reactive Flows*, 1st. Springer-Verlag Berlin Heidelberg, 2008, ISBN: 978-3-540-68622-4.

[32] M. V. Lurie, *Modeling of Oil Product and Gas Pipeline Transportation*. John Wiley & Sons, Inc., 2008, ISBN: 978-3-527-40833-7.

[33] M. E. Tuckerman, *Statistical mechanics : theory and molecular simulation*, eng. Oxford University Press, 2010, ISBN: 1-282-49066-4.

[34] F. M. White, *Viscous Fluid Flow*, 3rd. McGraw-Hill Education, 2019.

[35] J. Nocedal and S. Wright, *Numerical Optimization*, 2nd. Springer, 2006.

[36] D. Liberzon, *Calculus of Variations and Optimal Control Theory: A Concise Introduction*. Princeton University Press, 2012.

[37] A. E. Bryson and Y.-C. Ho, *Applied Optimal Control: Optimization, Estimation and Control*. Taylor & Francis Group, 1975.

[38] D. L. Powers, *Boundary Value Problems : And Partial Differential Equations*. 5th. Academic Press, 2006, ISBN: 9780125637381.

[39] R. A. Adams and C. Essex, *Calculus: A Complete Course*, 8th. Pearson, 2013, ISBN: 978 0 32 178107 9.

[40] M. Dandani, V. Lepiller, G. Abderrahmane, and P. Désévaux, "Numerical Visualizations of Mixing Enhancement in a 2D Supersonic Ejector," *Fluid Dynamics and Materials Processing*, vol. 14, pp. 23–37, Jan. 2018.

[41] The MathWorks, Inc. "ode45: Solve nonstiff differential equations — medium order method." (1994-2022), [Online]. Available: `https://se.mathworks.com/help/matlab/ref/ode45.html`. (Accessed: 28.03.2022).

[42] Y. A. Çengel and J. M. Cimbala, *Fluid Mechanics: Fundamentals and Applications*, 3rd. McGraw-Hill, 2014.

[43] The MathWorks, Inc. "fmincon: Find minimum of constrained nonlinear multivariable function." (1994-2022), [Online]. Available: `https://se.mathworks.com/help/optim/ug/fmincon.html`. (Accessed: 24.03.2022).

[44] R. Mudde, L. Deutz, V. Nievaart, and H. van Maanen, "LDA-Measurements of the Turbulence in and Around a Venturi," W. Rodi and M. Mulas, Eds., pp. 511–520, 2005.

[45] S. P. Vinod Chandavari, "Diffuser angle control to avoid slow separation," *International Journal of Technical Research and Applications*, vol. 2, pp. 16–21, 2014, ISSN: 2320-8163.

[46] H. Versteeg and W. Malalasekera, *An Introduction to Computational Fluid Dynamics: The Finite Volume Method*, 2nd. Pearson, 2007.

[47] The MathWorks, Inc. "trapz: Trapezoidal numerical integration." (1994-2022), [Online]. Available: `https://se.mathworks.com/help/matlab/ref/trapz.html`. (Accessed: 28.03.2022).

[48] The MathWorks, Inc. "bvp5c: Solve boundary value problem — fifth-order method." (1994-2022), [Online]. Available: `https://se.mathworks.com/help/matlab/ref/bvp5c.html`. (Accessed: 24.03.2022).

[49] The MathWorks, Inc. "Std: Standard deviation." (1994-2022), [Online]. Available: `https://se.mathworks.com/help/matlab/ref/std.html`. (Accessed: 28.03.2022).

[50] The MathWorks, Inc. "Spline: Cubic spline data interpolation." (1994-2022), [Online]. Available: `https://se.mathworks.com/help/matlab/ref/spline.html`. (Accessed: 31.03.2022).

[51] J. D. Anderson, *Fundamentals of Aerodynamics*, 6th. McGraw-Hill Education, 2017.

[52] S. B. Pope, *Turbulent Flows*. Cambridge University Press, 2000, ISBN: 9780521598866.

[53] F. Ornano, J. Braun, B. Saracoglu, and G. Paniagua, "Multi-stage nozzle-shape optimization for pulsed hydrogen–air detonation combustor," *Advances in Mechanical Engineering*, vol. 9, pp. 1–9, Feb. 2017.

[54] The MathWorks, Inc. “syms: Create symbolic scalar variables and functions, and matrix variables and functions.” (1994-2022), [Online]. Available: `https://se.mathworks.com/help/symbolic/syms.html`. (Accessed: 30.03.2022).

Appendix A

Additional Material

On request, the code implemented in MATLAB is available to the interested reader.

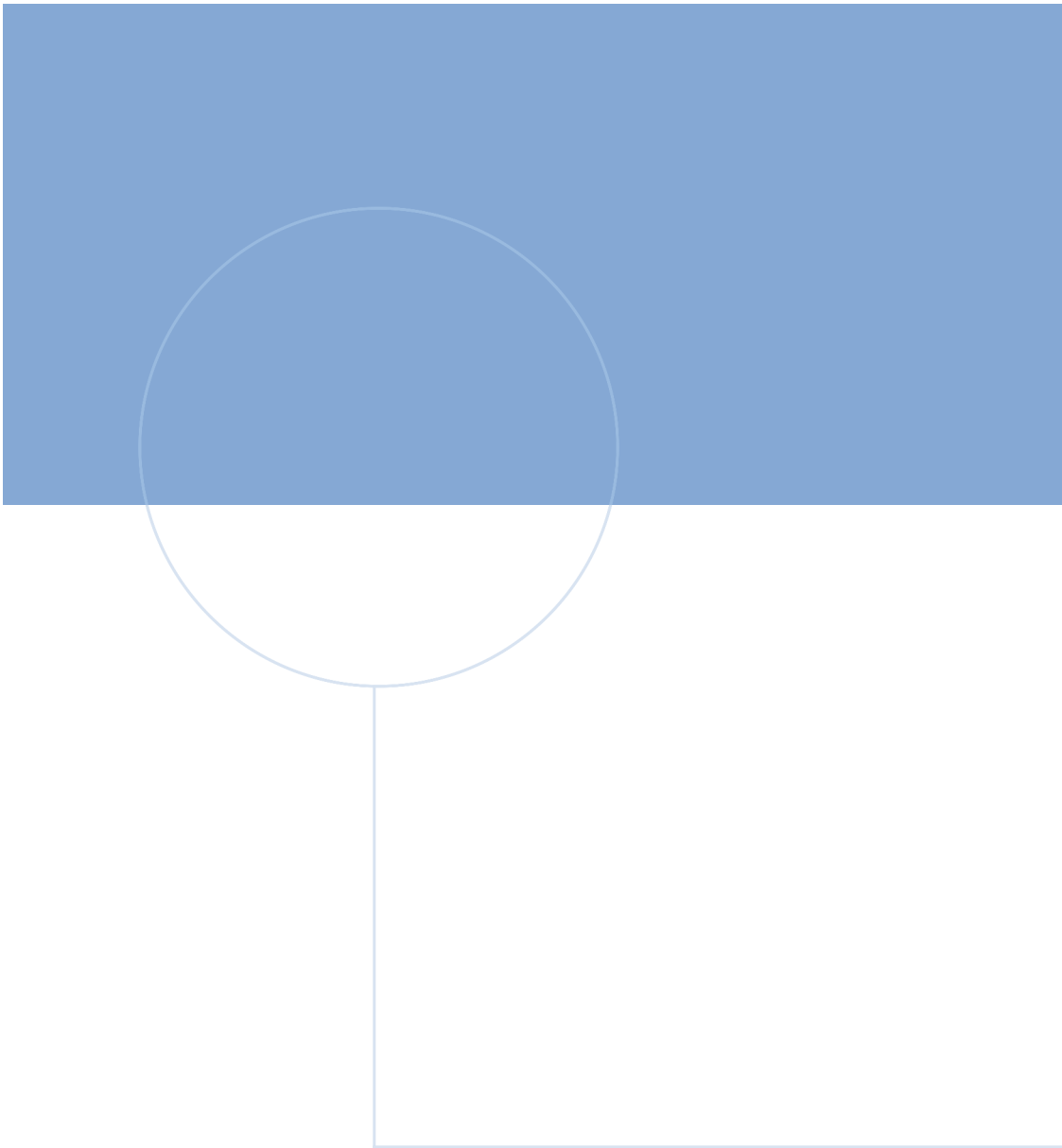

NTNU

Norwegian University of
Science and Technology